JOURNAL OF GEOPHYSICAL RESEARCH, VOL. 116, D23204, doi:10.1029/2011JD016283, 2011

On the effect of dust particles on global cloud condensation nuclei and cloud droplet number

V. A. Karydis,[1] P. Kumar,[2,3] D. Barahona,[4,5] I. N. Sokolik,[1] and A. Nenes[1,6]

Received 20 May 2011; revised 24 September 2011; accepted 26 September 2011; published 7 December 2011.

[1] Aerosol-cloud interaction studies to date consider aerosol with a substantial fraction of soluble material as the sole source of cloud condensation nuclei (CCN). Emerging evidence suggests that mineral dust can act as good CCN through water adsorption onto the surface of particles. This study provides a first assessment of the contribution of insoluble dust to global CCN and cloud droplet number concentration (CDNC). Simulations are carried out with the NASA Global Modeling Initiative chemical transport model with an online aerosol simulation, considering emissions from fossil fuel, biomass burning, marine, and dust sources. CDNC is calculated online and explicitly considers the competition of soluble and insoluble CCN for water vapor. The predicted annual average contribution of insoluble mineral dust to CCN and CDNC in cloud-forming areas is up to 40 and 23.8%, respectively. Sensitivity tests suggest that uncertainties in dust size distribution and water adsorption parameters modulate the contribution of mineral dust to CDNC by 23 and 56%, respectively. Coating of dust by hygroscopic salts during the atmospheric aging causes a twofold enhancement of the dust contribution to CCN; the aged dust, however, can substantially deplete in-cloud supersaturation during the initial stages of cloud formation and can eventually reduce CDNC. Considering the hydrophilicity from adsorption and hygroscopicity from solute is required to comprehensively capture the dust-warm cloud interactions. The framework presented here addresses this need and can be easily integrated in atmospheric models.

Citation: Karydis, V. A., P. Kumar, D. Barahona, I. N. Sokolik, and A. Nenes (2011), On the effect of dust particles on global cloud condensation nuclei and cloud droplet number, *J. Geophys. Res.*, *116*, D23204, doi:10.1029/2011JD016283.

1. Introduction

[2] Mineral dust is a major component of particulate matter in the atmosphere, accounting for more than 50% of the global aerosol load [*Grini et al.*, 2005; *Zender and Kwon*, 2005]. Mineral aerosol may be composed of iron oxides (e.g., hematite, goethite), carbonates (e.g., calcite, dolomite), quartz, and clays (e.g., kaolinite, illite, and montmorillonite) [*Chou et al.*, 2008; *Coz et al.*, 2009; *Lafon et al.*, 2006; *Twohy et al.*, 2009]. Differences in parent soils, and emission and transport processes cause substantial changes in size distribution, composition, and morphology of dust particles [*Jeong and Sokolik*, 2007; *Sokolik et al.*, 2001]. The long-range transport of dust particles can influence the composition and dynamic state of the atmosphere thousands of kilometers downwind of their source region [e.g., *Kallos et al.*, 2007; *Prospero et al.*, 2001]. Under favorable conditions, dust particles originating from Northern and Central Africa may be elevated and travel across the Atlantic Ocean toward the Caribbean [*Chiapello et al.*, 2005; *Kallos et al.*, 2006; *Karyampudi and Carlson*, 1988; *Karyampudi et al.*, 1999] or across the Mediterranean toward Europe, affecting both air quality and meteorology in Southern Europe [*Mitsakou et al.*, 2008; *Querol et al.*, 2009]. Dust from the Gobi and Taklamakan deserts often crosses the Pacific and reaches the west coast of the Americas [*Meskhidze et al.*, 2005a; *Meskhidze et al.*, 2003; *Sassen et al.*, 2002].

[3] Absorption of solar radiation by dust can modify the atmospheric thermodynamic structure, leading to suppression (or enhancement) of precipitation depending on cloud types and atmospheric conditions [*Yin and Chen*, 2007]. Moreover, dust particles are efficient ice nuclei (IN) and contribute to the formation of ice particles in cirrus and mixed-phase clouds [*DeMott et al.*, 2003; *Field et al.*, 2006; *Teller and Levin*, 2006; *Barahona et al.*, 2010a]. Dust may also interact with sea salt, anthropogenic pollutants, and secondary organic aerosol, forming particles that consist of a "core" of insoluble mineral dust with coatings of soluble material [*Gibson et al.*, 2007; *Levin et al.*, 2005; *Seisel et al.*, 2005].

[1]School of Earth and Atmospheric Sciences, Georgia Institute of Technology, Atlanta, Georgia, USA.
[2]School of Chemical and Biomolecular Engineering, Georgia Institute of Technology, Atlanta, Georgia, USA.
[3]Now at SABIC Innovative Plastics, Selkirk, New York, USA.
[4]NASA Goddard Space Flight Center, Greenbelt, Maryland, USA.
[5]Also at I.M. Systems, Inc., Rockville, Maryland, USA.
[6]Also at School of Chemical and Biomolecular Engineering, Georgia Institute of Technology, Atlanta, Georgia, USA.

0148-0227/11/2011JD016283

Dust particles with a soluble coating are typically very efficient cloud condensation nuclei (CCN), often maintaining their activity as IN [*Levin et al.*, 2005]. According to *Kelly et al.* [2007], small amounts of highly soluble components greatly enhance the ability of fine dust particles to serve as CCN. *Hoose et al.* [2008a] have shown that, depending on the dust mineralogical composition, coating with soluble material from anthropogenic sources can lead to quasi-deactivation of natural dust ice nuclei. Moreover, due to their large size, dust particles can act as giant CCN that can form efficient collector drops and initiate the onset of drizzle and precipitation [*Feingold et al.*, 1999; *Levin and Cotton*, 2009]. The same particles can strongly compete for water vapor in the nucleation zone of cloudy updrafts, potentially reducing supersaturation and cloud droplet formation [*Barahona et al.*, 2010b]. According to *Lee et al.* [2009], CCN concentration decreases in dusty regions up to 10–20% because dust competes for condensable H_2SO_4, reducing the condensational growth of ultrafine mode particles to CCN sizes. On the other hand, below 0.1% supersaturation, CCN concentrations increase significantly in dusty regions due to the presence of coarse dust particles. *Manktelow et al.* [2010] found that CCN-sized particles were depleted by an average of less than 5% during an extreme dust event over E. China, Korea, and Japan, because decreases in fine aerosols were mostly compensated for by increases in coarse particles.

[4] Köhler theory (KT), which is currently used to describe droplet formation in atmospheric models, assumes that the CCN activity of aerosols depends solely on their curvature and the fraction of soluble material. There is emerging evidence though that insoluble species (like freshly emitted mineral dust) can also act as good CCN even if they lack appreciable amounts of soluble material. *Koehler et al.* [2009] and *Herich et al.* [2009] measured CCN activation of two types of regional dust samples (Northern Africa and Arizona Test Dust) and several clays (kaolinite, illite, and montmorillonite) at atmospherically relevant supersaturations. The high CCN activity was attributed to soluble ions present in the material. Further analysis of these data by *Kumar et al.* [2009a] showed the importance of including water adsorption effects in describing the hygroscopic and CCN behavior of mineral aerosol. This was later confirmed by *Kumar et al.* [2011a, 2011b] who studied the CCN activity of dry- and wet-generated clays and mineral dusts representative of major regional dust sources (Northern Africa, East Asia/China, and Northern America). The observed hygroscopicity could not be attributed to the soluble ions present, but rather to the strong water vapor adsorption on the particle surface. *Lathem et al.* [2011] also demonstrated the importance of adsorption for describing the water uptake properties of volcanic ash. Finally, *Kumar et al.* [2011b] presented a "unified dust activation framework" to treat the activation of dust internally mixed with soluble salts by considering the effects of adsorption and absorption on water activity.

[5] The dependence of CCN activity on dry diameter differs between particles for which soluble material dominates their composition and those which lack any appreciable amounts of solute. This difference needs to be accounted for in calculation of CDNC when the CCN population contains both particle types. *Kumar et al.* [2009b] developed a cloud droplet formation parameterization to address this need, which accounts for the effect of adsorption activation by assuming the CCN constitute an external mixture of soluble aerosol (that follow KT) and completely insoluble aerosol (that follow FHH adsorption activation theory, FHH-AT). *Kumar et al.* [2011a] also developed a framework to treat dust particles with substantial amounts of soluble material where the CCN activity is influenced by both adsorption and solute.

[6] To date, global models and studies that include the dust impacts on cloud droplet number assume that dust acts as CCN only when soluble material exists in the particles (and controls its hygroscopicity) [e.g., *Hoose et al.*, 2008b; *Kelly et al.*, 2007; *Lee et al.*, 2009; *Manktelow et al.*, 2010; *Pringle et al.*, 2010a, 2010b; *Solomos et al.*, 2011]. Here we assess for the first time the impact of water adsorption on the CCN activity of insoluble (dust) aerosol and the resulting contribution to global CCN and cloud droplet number. Simulations are carried out with the NASA Global Modeling Initiative (GMI) Chemical Transport Model using offline wind fields and an online aerosol simulation coupled with the *Kumar et al.* [2009b] activation parameterization. The sensitivity of the proposed modeling framework to the size distribution and the adsorption parameters controlling the dust CCN activity is investigated. Finally, the sensitivity of our simulations to the deposition of solute on dust particles is addressed by extending the *Kumar et al.* [2009b] parameterization that enables us to include the "unified" adsorption-absorption activation theory of *Kumar et al.* [2011b] for describing the CCN activity of aged dust particles.

2. Model Description

2.1. NASA Global Modeling Initiative (GMI)

[7] The NASA GMI (https://gmi.gsfc.nasa.gov/gmi.html) is a modular 3-D chemistry and transport model (CTM), with the ability to carry out multiyear simulations for impact assessment studies. The detailed description of the framework is given by *Rotman et al.* [2001] and *Considine et al.* [2005]. The GMI aerosol model used in this study was contributed by *Liu et al.* [2005] and coupled to the GMI-CTM advection core. The aerosol module includes primary emissions, chemical production of sulfate in clear air and the in-cloud aqueous phase, gravitational sedimentation, dry deposition, wet scavenging in and below clouds, and hygroscopic growth. The model time step for chemistry is one hour. Model inputs include emissions of SO_2 (fossil fuel and natural), DMS, H_2O_2, black carbon (from biomass burning and fossil fuel), organic carbon (fossil fuel, biomass burning, and natural), mineral dust (four size bins), and sea salt (four size bins), which are provided by *Liu et al.* [2005]. The 2% (by mole) of fossil-fuel sulfur emission is assumed to occur as primary sulfate aerosol to account for the rapid conversion of SO_2 to SO_4^{2-} in combustion plumes. SO_2 emissions also include sources from sporadic and continuously emitting volcanoes (averaged over a 25-year time period). Biofuel emissions are categorized as fossil fuels.

[8] Dust aerosol fluxes at every 6 h were generated with the approach of *Ginoux et al.* [2001], using the NASA Goddard Data Assimilation Office (DAO) meteorological fields for year 1997. To account for a systematic overestimation in calculated AOD over deserts, *Liu et al.* [2005] reduced the submicron dust (0.1–1.25 μm bin) emission flux by roughly twofold. With this modified emissions

Table 1. Size Distribution Parameters Applied to Fossil Fuel, Biomass Burning, Marine, and Mineral Dust Aerosols

Aerosol Type	Aerosol Components	Density (g cm^{-3})	Median Diameter (μm)	Geometric Standard Deviation	Number Fraction	Reference
Fossil fuel	sulfate	1.77	0.1	1.9	1	*Chuang et al.* [1997]; *Radke et al.* [1988]
	organic carbon	1.2				
	black carbon	1.5				
Biomass burning	organic carbon	1.2	0.16	1.65	1	*Anderson et al.* [1996]
	black carbon	1.5				
Marine	natural sulfate	1.77	0.018	1.4	0.81	*Lance et al.* [2004]
	sea salt	2.2	0.075	1.6	0.18	
			0.62	2.7	0.01	
Mineral dust (base case)	mineral dust	2.6	0.16	2.1	0.93	*d'Almeida et al.* [1987]
			1.4	1.9	0.07	
			10	1.6	3×10^{-6}	
Mineral dust (sensitivity case)	mineral dust	2.6	0.18	1.8	0.76	*Chou et al.* [2008]
			0.7	1.4	0.13	
			1.5	2.0	0.11	

scheme, *Liu et al.* [2005] predicted a total dust flux (0.1–20 μm) of 1684 Tg yr^{-1}, which is on the lower end of predictions from ten different models (820–5102 Tg yr^{-1}). *Liu et al.* [2005] carried out an evaluation of the aerosol simulation against in situ observations from 15 oceanic sites. In regions of the southern hemisphere, which are influenced by dust emissions from Patagonian (Palmer Antarctic) and Australian (Cape Grim, Norfolk, New Caledonia) deserts, *Liu et al.* [2005] found that the model reproduces the seasonal cycle of dust concentration, although the dust concentration was underpredicted during the austral summer. In the Northern Hemisphere, the model reproduced the concentrations and seasonal cycles of the African dust sampled at Izaña Tenerife, Barbados, and Bermuda; the model overpredicted, however, the concentration in August at Izaña and underpredicted the concentration in July and August at Bermuda by a factor of two. Further details on the GMI framework can be found in *Barahona et al.* [2010a, 2011].

2.2. Aerosol Distribution

[9] The concentration of particles that can experience hygroscopic growth is given as an input from the aerosol module to the cloud droplet formation parameterization and is distributed in four aerosol types: fossil fuel (sulfate, organic mass, and black carbon), biomass burning (organic mass and black carbon), marine (natural sulfate and sea salt), and mineral dust. Fossil fuel, biomass burning, and marine aerosols are assumed to follow KT for CCN activation, whereas mineral dust is assumed to be insoluble and follow FHH-AT. Particles within each aerosol type are internally mixed and assumed to follow a prescribed number size distribution function (Table 1). Fossil fuel aerosols are represented by a size distribution given by *Chuang et al.* [1997] and *Radke et al.* [1988]. The particle size distributions for biomass burning aerosols are based on measurements by *Anderson et al.* [1996]. Marine aerosols are represented by a size distribution proposed by *Lance et al.* [2004] and mineral dust particles are assumed to follow the size distribution by *d'Almeida et al.* [1987]. The number concentration of each aerosol type (e.g., fossil fuel) is given by $N = m_{tot}/(V\rho_{tot})$, where m_{tot} is the total mass concentration (across size bins) of the aerosol type, V is the volume of a particle with dry diameter equal to d_g, and ρ_{tot} is the density of the aerosol type given by $\rho_{tot} = m_{tot} \Big/ \sum_{i=1}^{n} (m_i/\rho_i)$. Here m_i is the mass concentration of each component within the aerosol type (e.g., sulfate, OC, BC), ρ_i is its density, and n is the number of aerosol types.

2.3. Cloud Droplet Formation Parameterization

[10] Calculation of CDNC for particles following FHH-AT is performed in two conceptual steps, one involving the determination of the "CCN spectrum" (i.e., the number of CCN that can activate to form droplets at a certain level of supersaturation), and another one determining the maximum supersaturation, $s_{\max}$, that develops in the ascending cloudy parcels used to represent droplet formation in the general circulation model (GCM). The CDNC is then just the value of the CCN spectrum at $s_{\max}$.

[11] The "CCN spectrum," $F^s(s)$, is computed following *Kumar et al.* [2009b] and assumes that particles can be described either by KT or FHH-AT. $F^s(s)$ for an external mixture of lognormal particle size distributions is given by:

$$F^s(s) = \int_0^s n^s(s)ds = \sum_{i=1}^{n_m} \frac{N_i}{2} erfc\left[-\frac{\ln\left(\frac{s_{g,i}}{s}\right)}{x\sqrt{2}\ln(\sigma_i)}\right] \qquad (1)$$

where s is the level of water vapor supersaturation, $s_{g,i}$ is the critical supersaturation of the particle with a diameter equal to the geometric mean diameter of the mode i, σ_i is the geometric standard deviation for mode i, and x is an exponent that depends on the activation theory used. For modes following Köhler theory, $x = -3/2$ [*Fountoukis and Nenes*, 2005], while for particles following FHH theory, x depends on A_{FHH} and B_{FHH} [*Kumar et al.*, 2009b]. The adsorption parameter B_{FHH} expresses the long range interactions of adsorbed water layers with the dust surface. The smaller the value of B_{FHH}, the greater the distance from the dust surface for which attractive forces are present. A_{FHH} primarily represents the interaction between the first water monolayer and the dust surface. A_{FHH} and B_{FHH} are compound-specific and determined experimentally, with A_{FHH} typically ranging from 0.1–3.0, and B_{FHH} ranging from 0.5–3.0 [*Sorjamaa and Laaksonen*, 2007]. *Kumar et al.* [2011b] tested a wide range of fresh unprocessed regional dust samples and minerals and found that one set of the FHH parameters

(A_{FHH} = 2.25 ± 0.75, B_{FHH} = 1.20 ± 0.10) can adequately reproduce the measured CCN activity for all dust types considered.

[12] The maximum supersaturation, $s_{\max}$, in the ascending parcel is calculated from an equation that expresses the supersaturation tendency in cloudy air parcels, which at the point of maximum supersaturation becomes [*Barahona and Nenes*, 2007; *Nenes and Seinfeld*, 2003],

$$\frac{2aV}{\pi\gamma\rho_w} - Gs_{\max}I(0,s_{\max}) = 0 \quad (2)$$

where V is the updraft velocity, ρ_w is the density of water, and a, γ, G are parameters defined in *Barahona and Nenes* [2007]. Once $s_{\max}$ is determined by numerically solving equation (2), $N_d = F(s_{\max})$ from equation (1).

[13] In equation (2), $I(0,s_{\max})$ is known as the "condensation integral" [*Barahona and Nenes*, 2007; *Barahona et al.*, 2010b; *Kumar et al.*, 2009b] and it expresses the condensational depletion of supersaturation upon the growing droplets at the point of $s_{\max}$ in the cloud updraft. It is expressed as the sum of three terms [*Kumar et al.*, 2009b],

$$I(0,s_{\max}) = I_K(0,s_{\max}) + I_{FHH}(0,s_{\max}) + I_{GCCN}(0,s_{\max}) \quad (3)$$

The first term in the right hand side of equation (3) gives the contribution from particles that follow Köhler theory, $I_K(0,s_{\max})$, the second one from particles that follow the FHH theory, $I_{FHH}(0,s_{\max})$, and the third one accounts for the effect of the very large and giant CCN (neglected by the other two terms). Using the population splitting approach of *Nenes and Seinfeld* [2003], $I_K(0,s_{\max})$ is calculated as: $I_K(0,s_{\max}) = I_{K,1}(0,s_{part}) + I_{K,2}(s_{part},s_{\max})$, where $I_{K,1}(0,s_{part})$ and $I_{K,2}(s_{part},s_{\max})$ are presented by *Fountoukis and Nenes* [2005] or *Kumar et al.* [2009b]. The partition supersaturation, s_{part}, separates two CCN populations, one (expressed by $I_{K,2}(s_{part},s_{\max})$) for which droplets experience negligible growth beyond the critical diameter ($s_c \approx s_{\max}$), and another one (expressed by $I_{K,1}(0,s_{part})$) for which droplet growth is much larger than the critical diameter ($s_c \ll s_{\max}$). In equation (3), $I_{FHH}(0,s_{\max})$ represents the contribution of FHH particles to the condensation integral [*Kumar et al.*, 2009b].

[14] If dust particles contain a substantial fraction of soluble material, the critical supersaturation is determined using the "unified dust activation framework" of *Kumar et al.* [2011b], which involves determining the maximum of the relevant equilibrium curve describing an aerosol particle (consisting of insoluble core with a soluble coating) in equilibrium with the surrounding water vapor:

$$s = \frac{4\sigma M_w}{RT\rho_w D_P} - \frac{\varepsilon_s D_{dry}^3 \kappa}{\left(D_P^3 - \varepsilon_i D_{dry}^3\right)} - A_{FHH}\left(\frac{D_P - \varepsilon_i^{1/3} D_{dry}}{2D_w}\right)^{-B_{FHH}} \quad (4)$$

where D_p is the wet equilibrium diameter, D_{dry} is the particle dry diameter, ε_i is the insoluble volume fraction, ε_s is the soluble volume fraction, and κ is the hygroscopicity of the soluble fraction. The exponent x in the case of aged dust particles lies somewhere between the KT and FHH-AT limits, and is determined (as described by *Kumar et al.* [2011b]) by performing a power law fit between s_c and D_{dry} determined from equation (4). Given that dust is considered to be a separate population from other aerosol types, application of the unified dust activation framework in the *Kumar et al.* [2009b] parameterization is carried out by replacing the x, s_c normally computed by FHH-AT with those of the unified framework.

[15] Finally, $I_{GCCN}(0,s_{\max})$ accounts for the effect of the very large and giant CCN on the condensation rate and is presented by *Barahona et al.* [2010b] as:

$$I_{GCCN}(0,s_{\max}) = \sum_{i=1}^{n_m}\left(\frac{N_i}{2}D_{g,i}\exp\left[\left(\frac{x}{\sqrt{2}}\right)^2 \ln^2\sigma_i\right] \cdot erfc\left(-\frac{1}{x\sqrt{2}\ln\sigma_i}\ln\frac{D_{p_{\min}}}{D_{g,i}} + \frac{x}{\sqrt{2}}\ln\sigma_i\right)\right) \quad (5)$$

where $D_{p_{\min}}$ is the wet equilibrium diameter of the smallest particle that activates (i.e., for which $s_c = s_{\max}$) and $D_{g,i}$ is the geometric mean diameter of mode i. For giant nuclei following Köhler theory, $D_{p_{\min}} = 2A/(3\sqrt{3}s_{part})$, where $A = 4\sigma M_w/RT\rho_w$, and represents the boundary between particles that experience significant growth after activation and those that are strongly kinetically limited [*Barahona et al.*, 2010b; *Nenes and Seinfeld*, 2003]. Giant nuclei following FHH theory do not grow significantly after activation and therefore are kinetically limited by the inertial mechanism [*Nenes et al.*, 2001]; indeed, $D_c/D_{dry} < 2$ for most atmospherically relevant combinations of A_{FHH} and B_{FHH} [*Kumar et al.*, 2009b], where D_c is the critical wet droplet diameter. $D_{p_{\min}}$ is calculated at s_{part}, given by the solution of equation (4).

2.4. Model Application

[16] The model results presented here are based on 1 yr simulations and the first month of each simulation has been excluded in order to limit the effect the initial conditions have on the results (simulations with longer startup periods did not substantially affect the simulation results). The meteorological fields used in the simulations were taken from the Goddard Institute for Space Studies version II (GISS II) GCM [*Koch and Rind*, 1998; *Rind and Lerner*, 1996], which includes a slab (Q-flux) ocean model to represent the ocean-atmospheric coupling. The data set spans over 1 yr and represents the period from March 1997 to February 1998. The horizontal resolution is 4° latitude by 5° longitude. The vertical resolution is 23 vertical layers (from surface to 0.017 hPa). Meteorological information was updated at 3 h intervals and archived for the year of simulation.

[17] Parameters used by the cloud droplet formation parameterization in this study include the aerosol size distributions (section 2.1), an effective water vapor uptake coefficient of 0.06 [*Fountoukis et al.*, 2007], the updraft velocity representative of typical stratocumulus clouds and constrained using observations, $V = 0.3$ m s^{-1} over land, and $V = 0.15$ m s^{-1} over ocean [*Chuang et al.*, 2000; *Guibert et al.*, 2003; *Meskhidze et al.*, 2005b], and "base case" FHH adsorption parameters, A_{FHH} = 2.25 and B_{FHH} = 1.2 [*Kumar et al.*, 2011b]. Updraft velocity varies significantly within a GCM grid cell and between clouds; however, grid-average CDNC for stratiform clouds can be calculated by computing CDNC at a "characteristic" vertical velocity

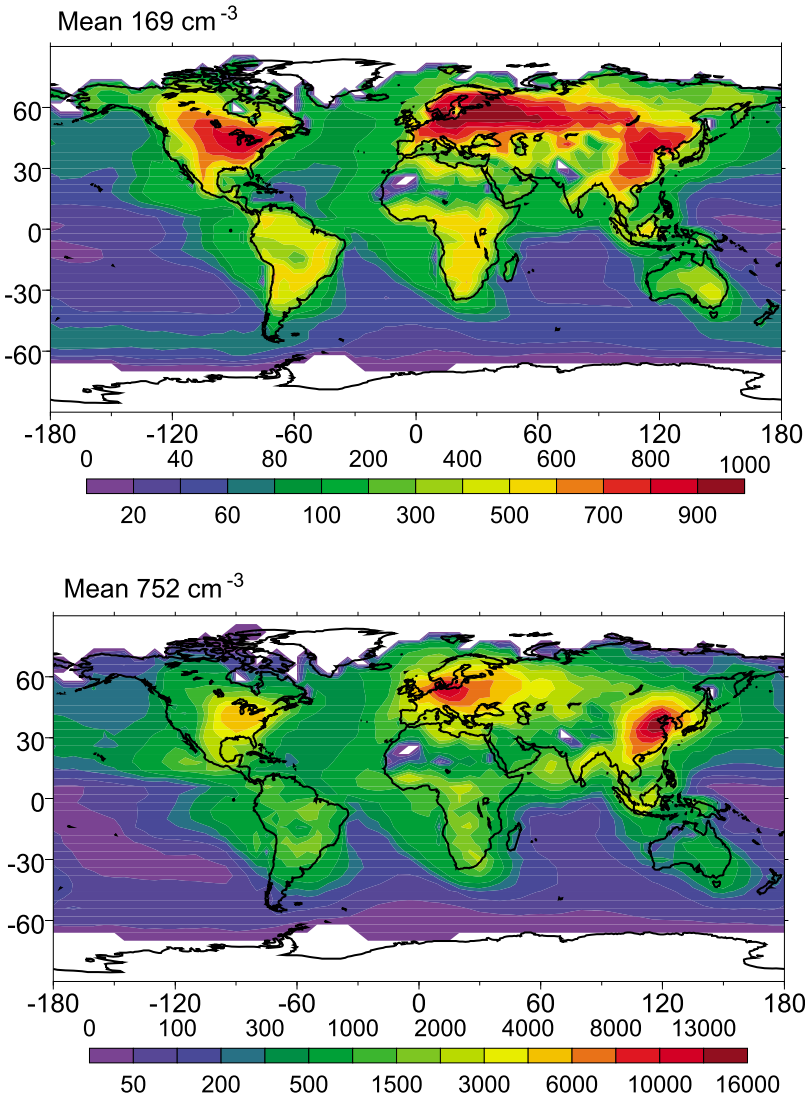

Figure 1. Predicted annual (top) mean cloud droplet and (bottom) cloud condensation nuclei (CCN) at 0.2% supersaturation concentrations (cm^{-3}) for the lowest cloud-forming level (960 mbar). White represents cloud-free areas.

[*Morales and Nenes*, 2010], which is very close to the average updraft velocity. *Meskhidze et al.* [2005b] and *Fountoukis et al.* [2007] showed that using the average updraft gives optimal CDNC closure in cumulus and stratocumulus clouds sampled in a variety of field campaigns.

3. Results

3.1. Overview of Model Predictions

[18] The predicted annual mean CCN at 0.2% supersaturation and cloud droplet number concentrations for the lowest cloud-forming level (at 960 mbar) are shown in Figure 1. CDNC is referred to the number concentration of droplets nucleated in-cloud and represents an upper limit since the model does not account for droplet depletion by collision, coalescence and collection. As expected, higher CDNC concentrations (up to 1000 cm^{-3}) are predicted over the midlatitudes of the Northern Hemisphere (i.e., over China, Europe, and eastern U.S.; Figures 1a and 2), consistent with the high concentration levels of CCN associated with industrialized regions (Figure 1b). Over the continents of the Southern Hemisphere, large CDNC values (up to 600 cm^{-3}) occur over regions affected by biomass burning in South America and Africa. The lower continental CDNC values are predicted over the arid areas of the Sahara and Gobi deserts (up to 300 cm^{-3}). Over oceans, CDNC is increased up to 300 cm^{-3} by continental aerosol transported by the trade winds off the subtropical west coasts of Africa and America, and westerlies in midlatitude east coasts of North America and Asia (Figure 1) [*Minnis et al.*, 1992; *Prospero et al.*, 1983]. In contrast to the Northern Hemisphere, lower cloud droplet number concentrations are found over the cleaner remote oceans of the Southern Hemisphere and in the polar regions (Figure 1a, 1b). In these regions, CDNC is predicted to be up to 40 cm^{-3}. Over the Southern Ocean, larger CDNC values are predicted (up to 80 cm^{-3}) due to the enhanced production of sulfate from dimethyl sulfide (DMS) oxidation, and the high concentrations of sea salt, which is lofted by winds associated with the Antarctic

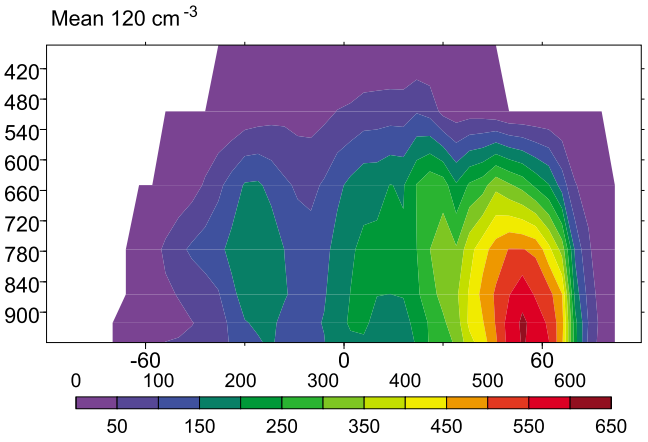

Figure 2. Predicted zonal annual mean cloud droplet number concentration (cm^{-3}). White areas correspond to non-cloud-forming regions.

circumpolar vortex that flows eastward around Antarctica. Predicted CDNC decreases with altitude over the polluted areas of the Northern Hemisphere caused by a decrease in aerosol concentration (Figure 2). Over the tropics, however, CDNC increases until 865 mbar, influenced by long-range transport of polluted air masses, and then decreases. The global mean CDNC is predicted to be 169 cm^{-3}, 177 cm^{-3}, 188 cm^{-3}, 181 cm^{-3}, and 128 cm^{-3} at 960, 920, 865, 780, and 650 mbar, respectively. These values are within the limits of simulated CDNC published in the literature. *Merikanto et al.* [2010] obtained a yearly global average CDNC of 211–240 cm^{-3} from model runs at 300–1000 m above ground level. *Chen et al.* [2010] reported a CDNC value of 189 cm^{-3} at 972 mbar and 122 cm^{-3} at 850 mbar. *Penner et al.* [2006] found the CDNC ranging from 119 cm^{-3} to 159 cm^{-3} near 850 mbar. *Barahona et al.* [2011] found the global mean CDNC ranging from 96 cm^{-3} to 103 cm^{-3} at 850 mbar depending on the climatological meteorological fields used. Finally, *Leibensperger et al.* [2011] report a global mean CDNC of 83 cm^{-3} at 850 mbar.

3.2. Model Evaluation

[19] The predicted cloud droplet number concentration is compared against observational data from continental, polluted marine, and clean marine regions around the world (Figure 3). The predictions reflect aerosol distributions in an average climate state; given that the observations span over a decade, we expect a spatial and seasonal correspondence with the predictions. The summary of this comparison is depicted in Table 2 and Figure 4. Over clean marine regions,

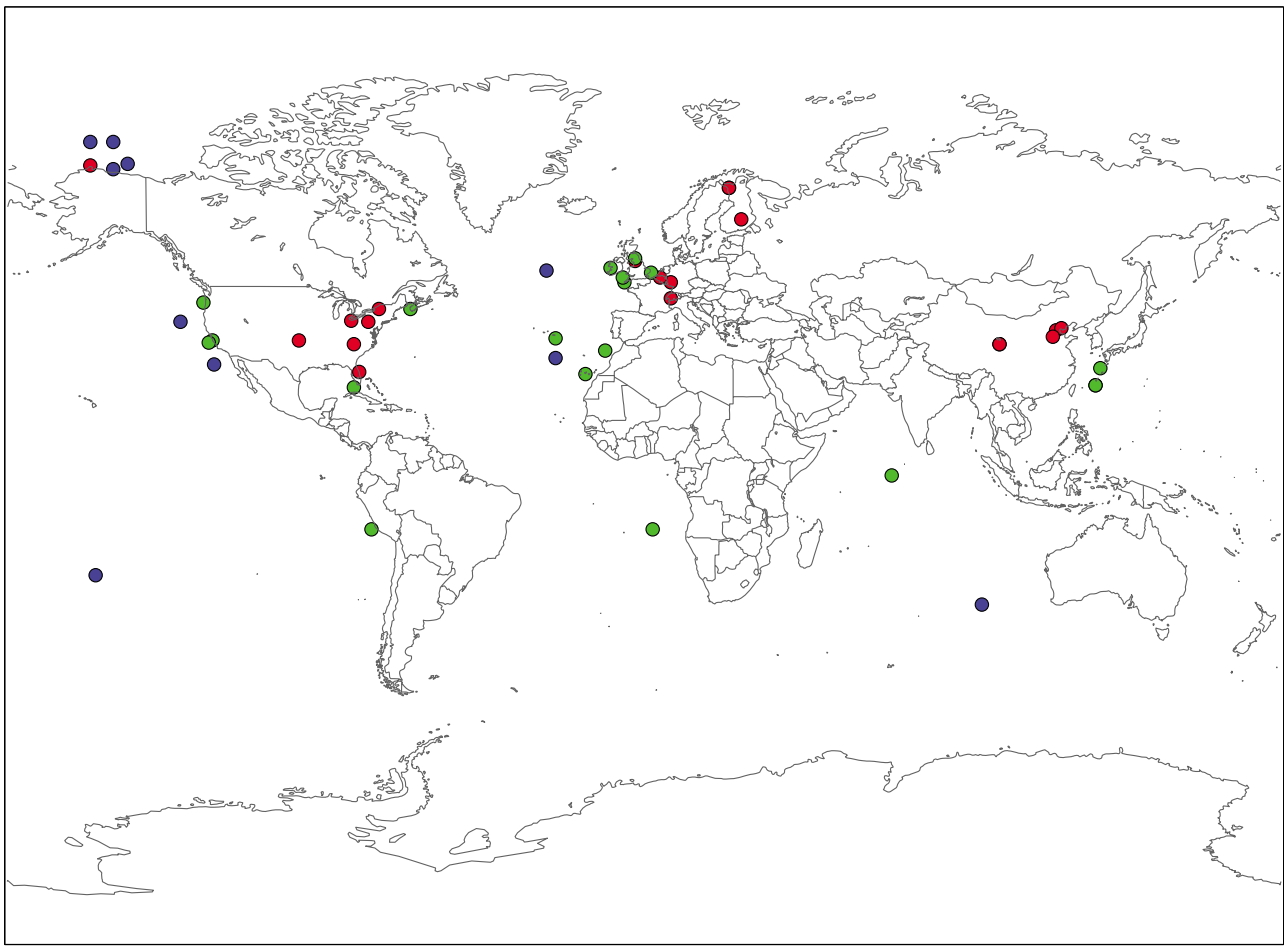

Figure 3. Location of observational data used for the evaluation of model predictions. Continental, polluted marine, and clean marine regions are represented by red, green, and blue symbols, respectively.

Table 2. Comparison of Simulated and Observed Global Cloud Droplet Number Concentrations

Location	Latitude	Longitude	Time	Observation	Simulation	Reference
South Pacific Ocean			Jul 2002 to Dec 2004	40	27	*Bennartz* [2007]
South Pacific Ocean	20S–35S	135W–175W	1982–2009	82	27	*Rausch et al.* [2010]
Eastern Pacific Ocean	29N–32N	120W–123W	Jul 2001	49–279	108	*Straub et al.* [2007]; *vanZanten et al.* [2005]
North Pacific Ocean	41N	131W	Apr 2004	21–74	91	*Wilcox et al.* [2006]
North Pacific Ocean			Jul 2002 to Dec 2004	64	60	*Bennartz* [2007]
Atlantic Ocean (west of Canary Islands and south of Azores Islands)	32N	25W	Jul 2001	17	49	*Schuller et al.* [2005]
North Atlantic Ocean			Jul 2002 to Dec 2004	89	90	*Bennartz* [2007]
South Atlantic Ocean			Jul 2002 to Dec 2004	67	56	*Bennartz* [2007]
South Indian Ocean			Jul 2002 to Dec 2004	42	33	*Bennartz* [2007]
West Australia (remote)	30S–40S	88E–103E	1982–2009	107	41	*Rausch et al.* [2010]
Beaufort Sea (western Arctic Ocean)	72N–78N	154W–159W	Jun 1980	178–365	158	*Herman and Curry* [1984]
Beaufort Sea (western Arctic Ocean)	70.5N–73N	145N-147N	Jun 1995	20–225	183	*Hobbs and Rangno* [1998]
Beaufort Sea (western Arctic Ocean)	65N–75N	130W–170W	Apr 1998	48–77	182	*Gultepe and Isaac* [2002]; *Gultepe et al.* [2004]
Northeastern Alaskan coast	69N–71N	150W–158W	Oct 2004	10–30	200	*Luo et al.* [2008]
Yellow Sea (eastern coast of China)	28N–31N	127E–131E	2001–2003	30–1000	226	*Zhao et al.* [2006]
South East Asia coast	10N–40N	105E–150E	1982–2009	186 (100–250)	263	*Rausch et al.* [2010]
North East Asia coast			Jul 2002 to Dec 2004	129	263	*Bennartz* [2007]
North America coast (Pacific Ocean)			Jul 2002 to Dec 2004	96	124	*Bennartz* [2007]
North America coast (Pacific Ocean)	15N–35N	115W–140W	1982–2009	159 (150–300)	124	*Rausch et al.* [2010]
South America coast (Pacific Ocean)			Jul 2002 to Dec 2004	77	210	*Bennartz* [2007]
South America coast (Pacific Ocean)	8S–28S	70W–90W	1982–2009	182 (100–300)	210	*Rausch et al.* [2010]
North Africa coast (Atlantic Ocean)			Jul 2002 to Dec 2004	95	113	*Bennartz* [2007]
South African coast (Atlantic Ocean)			Jul 2002 to Dec 2004	95	161	*Bennartz* [2007]
South African coast (Atlantic Ocean)	5S–25S	10W–15E	1982–2009	153 (130–300)	161	*Rausch et al.* [2010]
Eastern North Atlantic Ocean	50N–55N	25W–30W	Apr 1987	65–300	88	*Harshvardhan et al.* [2002]
Northwest coast of Santa Maria, Azores	37N	25W	Jun 1992	150 (74–192)	240	*Dong et al.* [1997]
Canary Islands vicinity	28N	16.5W	Jun–Jul 1997	51–256	167	*Brenguier et al.* [2003]; *Chuang et al.* [2000]
Atlantic Ocean (west of Morocco)	34N	11W	Jul 2001	77	196	*Schuller et al.* [2005]
Coast of Oregon	45.5N	124.5W	Aug 1992	25–210	120	*Hoppel et al.* [1994]
Key West, Florida	24.5N	82W	Jul 2002	186–2409	123	*Meskhidze et al.* [2005b]
Bay of Fundy, Nova Scotia, Canada	44N	66W	Aug 1995	61 (59–97)	280	*Gultepe et al.* [2001]
Cornwall Coast (southwestern UK)	50N	5.5W	Feb 2001	130	112	*Di Giuseppe* [2005]
British Isles, UK	55N	2.5W	Apr 1993	172	338	*Ekman* [2002]
British Isles, UK	51N	6W	Oct 1993	119	173	*Ekman* [2002]
British Isles, UK	53N	9.5W	Dec 1993	96	129	*Ekman* [2002]
Southeastern coast of England	51.5N–52N	1.5E–2.5E	Sep 2005	151–249	580	*Romakkaniemi et al.* [2009]
Indian Ocean (southwest of India)	10S–10N	65E–75E	Feb–Mar 1999	100–500	161	*Liu et al.* [2003]
Qinghai Province (western China)	34N–37N	98E–103E	2001–2004	30–700	577	*Zhao et al.* [2006]
Beijing, China	37N–41N	113E–120E	2004–2005	30–1100	772	*Zhao et al.* [2006]
Northeastern China (east of Beijing)	39N–40N	117.5E–118.5E	Apr–May 2006	200–800	610	*Ma et al.* [2010]
Hebei Province (central eastern China)	35N–40N	112E–119E	1990–1993	30–400	637	*Zhao et al.* [2006]
Cumbria, northern England	54.5N	2.5W	Mar–Apr 1995	100–2000	396	*Bower et al.* [1999]
Cumbria, northern England	54.5N	2.5W	May 1993	482–549	562	*Bower et al.* [1997]
Koblenz, Germany	50N	7.5E	May 2005	675–900	804	*Lehmann et al.* [2009]
Koblenz, Germany	50N	7.5E	Oct 2006	965	956	*Lehmann et al.* [2009]
Northern Finland	68N	24E	Apr 2000–Feb 2002	154 (30–610)	550	*Komppula et al.* [2005]
Kuopio, Finland	62.5N	27.5E	Oct–Nov 2006 Aug–Sep 2007 Sep–Oct 2008	138	899	*Portin et al.* [2009]
Northern Finland	68N	24E	Oct–Nov 2004	55–470	700	*Lihavainen et al.* [2008]

Table 2. (continued)

Location	Latitude	Longitude	Time	Observation	Simulation	Reference
Cabauw, Netherlands	51N	4.5E	May 2008	180–360	660	*Henrich et al.* [2010]
Jungfraujoch, Switzerland	46.5N	7.5E	Jul–Aug 2000	112–416	706	*Henning et al.* [2002]
Barrow, Alaska	71.5N	156.5W	Aug 2000	56	201	*Dong and Mace* [2003]
Barrow, Alaska	71.5N	156.5W	May 2000	222	365	*Dong and Mace* [2003]
Barrow, Alaska	71.5N	156.5W	Jun 2000	121	281	*Dong and Mace* [2003]
Barrow, Alaska	71.5N	156.5W	Jul 2000	54	238	*Dong and Mace* [2003]
Barrow, Alaska	71.5N	156.5W	Sep 2000	81	280	*Dong and Mace* [2003]
Southern Great Plains, Oklahoma	36.5N	97.5W	winter 1997–2002	265–281	896	*Dong et al.* [2005]
Southern Great Plains, Oklahoma	36.5N	97.5W	winter 1996–1998	244	896	*Dong et al.* [2000]
Southern Great Plains, Oklahoma	36.5N	97.5W	spring 1997–2002	200–219	710	*Dong et al.* [2005]
Southern Great Plains, Oklahoma	36.5N	97.5W	spring 1996–1998	203	710	*Dong et al.* [2000]
Southern Great Plains, Oklahoma	36.5N	97.5W	summer 1997–2002	128–159	617	*Dong et al.* [2005]
Southern Great Plains, Oklahoma	36.5N	97.5W	summer 1996–1998	131	617	*Dong et al.* [2000]
Southern Great Plains, Oklahoma	36.5N	97.5W	autumn 1997–2002	217–249	730	*Dong et al.* [2005]
Southern Great Plains, Oklahoma	36.5N	97.5W	autumn 1996–1998	276	730	*Dong et al.* [2000]
Southern Great Plains, Oklahoma	36.5N	97.5W	Mar 2000	200 (100–320)	761	*Iacobellis and Somerville* [2006]
Southern Great Plains, Oklahoma	36.5N	97.5W	Apr 1994	650	726	*Dong et al.* [1997]
Southern Great Plains, Oklahoma	36.5N	97.5W	Sep–Oct 1995	457	712	*Dong et al.* [1997]
Cleveland, Ohio; Detroit, Michigan	40N–42.5N	80.5W–85W	Aug 2004	320–1300	690	*Fountoukis et al.* [2007]
Central Ontario, Canada	50N	85W	Oct 1995	147 (119–173)	605	*Gultepe et al.* [2001]
Central Ontario	50N	85W	summer 1988; 1982	350–360	533	*Leaitch et al.* [1992]
Central Ontario	50N	85W	winter 1984	190	854	*Leaitch et al.* [1992]
Upper New York State	44N	75W	autumn 1984	240	780	*Leaitch et al.* [1992]
State College, Pennsylvania	41N	78W	Oct 1996	388	817	*Dong et al.* [1998]
Mount Gibbes, North Carolina	35.5N	82W	1993–1995	238–754	570	*Menon et al.* [2002]; *Saxena et al.* [1996]
Cape Kennedy, Florida	28.5N	80.5W	Aug 1995	250–330	213	*Burnet and Brenguier* [2007]

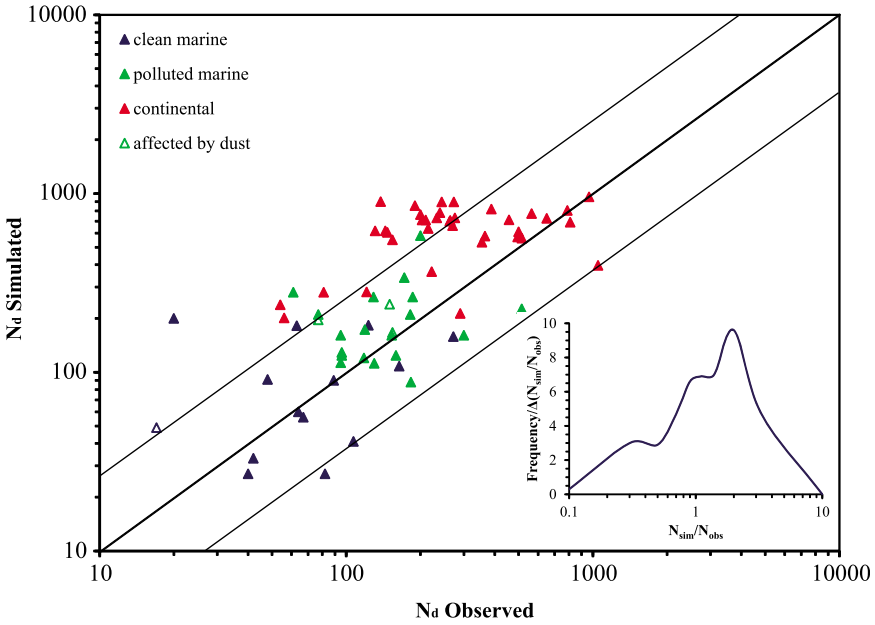

Figure 4. Comparison of simulated and observed global cloud droplet number concentrations (cm^{-3}). Open symbols correspond to dust affected regions. Also shown are the 1:1, ±50% lines, and the probability distribution of the ratio of the simulated CDNC to the observed CDNC (inset plot).

concentrations of 27 cm^{-3} (South Pacific) to 108 cm^{-3} (Eastern Pacific) are predicted; this agrees with retrieved CDNC values mostly to within 50%, ranging from 40 cm^{-3} (South Pacific [*Bennartz*, 2007]) to 279 cm^{-3} (Eastern Pacific [*Straub et al.*, 2007; *vanZanten et al.*, 2005]). Larger underestimation is found over the remote area west of Australia (41 cm^{-3} versus 107 cm^{-3} reported by *Rausch et al.* [2010]). Moreover, over the Western Arctic Ocean, the predicted CDNC range from 158 cm^{-3} to 200 cm^{-3}. This agrees well with available observations [*Herman and Curry*, 1984; *Hobbs and Rangno*, 1998], but is considerably overpredicted over the North Pacific and Arctic Ocean [*Gultepe and Isaac*, 2002; *Gultepe et al.*, 2004; *Luo et al.*, 2008].

[20] The predicted CDNC increases to 88–580 cm^{-3} over polluted marine regions close to coasts. The highest observed CDNC value is over the Yellow Sea (eastern coast of China). In particular, *Zhao et al.* [2006] reported measured values ranging from 30 cm^{-3} to 1000 cm^{-3}. The predicted CNDC is 226–263 cm^{-3} which is relatively high compared to satellite retrievals (100–250 cm^{-3} reported by *Bennartz* [2007] and *Rausch et al.* [2010]). The model predictions are in better agreement with these studies over North America coast (124 cm^{-3} versus 96–300 cm^{-3}), South America coast (210 cm^{-3} versus 77–300 cm^{-3}), and Africa (113–161 cm^{-3} versus 95–300 cm^{-3}). Over Atlantic Ocean, the CDNC predictions range between 88 cm^{-3} (eastern north Atlantic) and 240 cm^{-3} (Santa Maria, Azores). This is well within the observed values over that region (65–300 cm^{-3} [*Brenguier et al.*, 2003; *Chuang et al.*, 2000; *Dong et al.*, 1997; *Harshvardhan et al.*, 2002; *Schüller et al.*, 2005]).

[21] The predicted CDNC over continental regions ranges between 201 cm^{-3} (Barrow, AK) and 956 cm^{-3} (Koblenz, Germany) compared to observed values of up to 2000 cm^{-3} (Cumbria, North England [*Bower et al.*, 1999]). In Asia, predicted values range from 577 cm^{-3} over Western China (observed 30–700 cm^{-3} [*Zhao et al.*, 2006]) to 772 cm^{-3} over Beijing (observed 30–1000 cm^{-3} [*Zhao et al.*, 2006]). In Europe, the model predicts a lower concentration (396 cm^{-3}) over North England, where there are the highest observations (100–2000 cm^{-3} [*Bower et al.*, 1999]). The highest CDNC are predicted over Koblenz, Germany (804–956 cm^{-3}) and are in good agreement with observations (675–965 cm^{-3} [*Lehmann et al.*, 2009]). Over Finland, the model tends to overpredict CDNC, with values ranging from 550 cm^{-3} to 899 cm^{-3} versus 30 cm^{-3} to 610 cm^{-3} [*Komppula et al.*, 2005; *Lihavainen et al.*, 2008; *Portin et al.*, 2009]. Finally, over North America, the predicted CDNC range from 201 cm^{-3} over Alaska (observed of 54–222 cm^{-3} [*Dong and Mace*, 2003]) to 896 cm^{-3} over Oklahoma (observed of 100–650 cm^{-3} [*Dong et al.*, 2005, 1997, 2000; *Iacobellis and Somerville*, 2006]). The observations range from 54 cm^{-3} (Barrow, AK [*Dong and Mace*, 2003]) to 1300 cm^{-3} (Cleveland, OH, and Detroit, MI [*Fountoukis et al.*, 2007]).

[22] Overall, the model is in reasonably good agreement with observations over both clean and polluted marine regions as well as over regions that are relatively close to dust sources (e.g., Canary Islands). More precisely, 67% of the CDNC predictions over those regions diverge less than 50% from available measurements (Figure 4). The model tends to overpredict the CDNC compared to observed data from continental regions (Figure 4). Considering the influence of droplet collision and coalescence processes may, in part, reduce prediction biases. Given however that dust is not expected to be a significant contributor to CCN number in these regions, we do not anticipate the overprediction bias to affect conclusions.

3.3. Effect of Dust on CCN and CDNC

[23] The contribution of insoluble particles to cloud droplet formation is potentially most important in areas close to mineral dust sources. These areas may not always be associated with extensive cloud cover; to account for this,

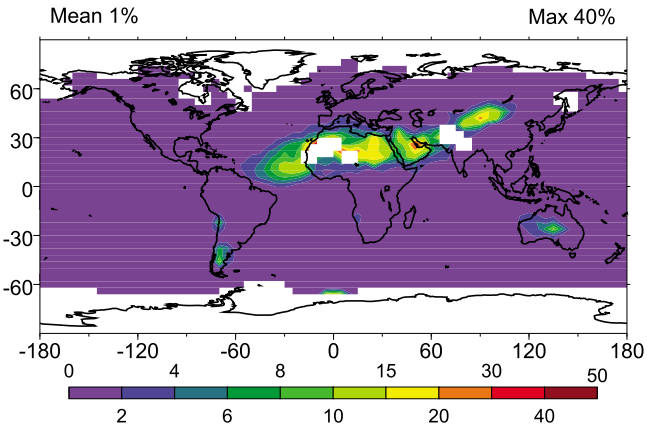

Figure 5. Predicted annual mean contribution (%) of mineral dust to particle number concentrations for the lowest cloud-forming level (960 mbar). White represents areas that are free of warm clouds throughout the year.

CDNC are calculated only in cells for which warm clouds are present (i.e., cloud water is present, and cloud top temperature exceeds 263K). Mineral dust effects on CDNC depend on the predicted contribution of mineral dust to total aerosol number concentration, as the available aerosol budget is the main factor driving the CCN population. Close to deserts, the dominant aerosol constituent (80–99% by mass) is mineral dust with the rest of the aerosols consisting of soluble materials, such as sulfate, organic carbon, and sea salt from long-range transport. However, these soluble aerosols are small in size compared to mineral dust and therefore can contribute substantially to aerosol number and CCN concentrations. The predicted contribution of mineral dust to particle number concentrations is presented in Figure 5. The contribution of dust to the total aerosol number concentration is small on a global scale (~1%), but regionally can be large, especially during dust episodes and their long-range transport (Figure 5). The largest contribution (up to 40%) is seen over North Africa and Asia (Arabian Peninsula and Gobi Desert) while mineral dust from South America (Patagonian Desert) and Australian deserts also contributes to the total aerosol number concentration (10–15%). These contributions represent an average climatology but will vary significantly, both seasonally and interannually.

[24] To investigate the potential importance of dust on cloud droplet formation, the predicted contribution of dust to total CCN is shown in Figure 6 for moderate (0.2%) and high (0.4%) supersaturations. The contribution of mineral dust to the CCN concentration decreases with decreasing supersaturation as insoluble aerosols are less hygroscopic and they need higher supersaturations in order to activate compared to soluble particles. Nevertheless, dust particles are coarser than soluble aerosols and therefore, if coated with hygroscopic material, they can potentially activate at lower supersaturations than smaller anthropogenic particles. At 0.2% supersaturation, the contribution of mineral dust to the total CCN concentration is up to 30% while at 0.4% supersaturation the contribution increases to 35%. In both cases, the maximum predicted contribution occurred on the eastern part of the Arabian Peninsula.

[25] The contribution of dust to CNDC is computed directly from the parameterization output, as the activation fraction for each aerosol mode is known. The predicted s_{max} in clouds forming in these dusty areas remains low (~0.1% on average), hence mineral dust contributes up to 23.8% of the CDNC (Figure 7). Moreover, allowing dust to act as CCN resulted in a relatively significant decrease of s_{max} over Western Saharan (30%) and Patagonian (10%) deserts. Over the remaining arid areas (e.g., Gobi and Australian deserts) the decrease in s_{max} is less important (less than 5%). Mineral dust also has a small contribution to the annual average predicted CDNC across the Atlantic Ocean, as far as the Caribbean Sea (up to 10% near the North African coast). This contribution can be significantly larger during dust episodes. The peak contribution of mineral dust to CDNC across the Atlantic Ocean is predicted during the month of February (15%). The greatest seasonal variability of the contribution of mineral dust to CDNC is predicted downstream of the Patagonia Desert, where it varies from 2% during May to 40% during February.

4. Sensitivity Analyses

[26] Dust-relevant inputs in the CDNC parameterization, other than dust concentration, include A_{FHH}, B_{FHH} and the

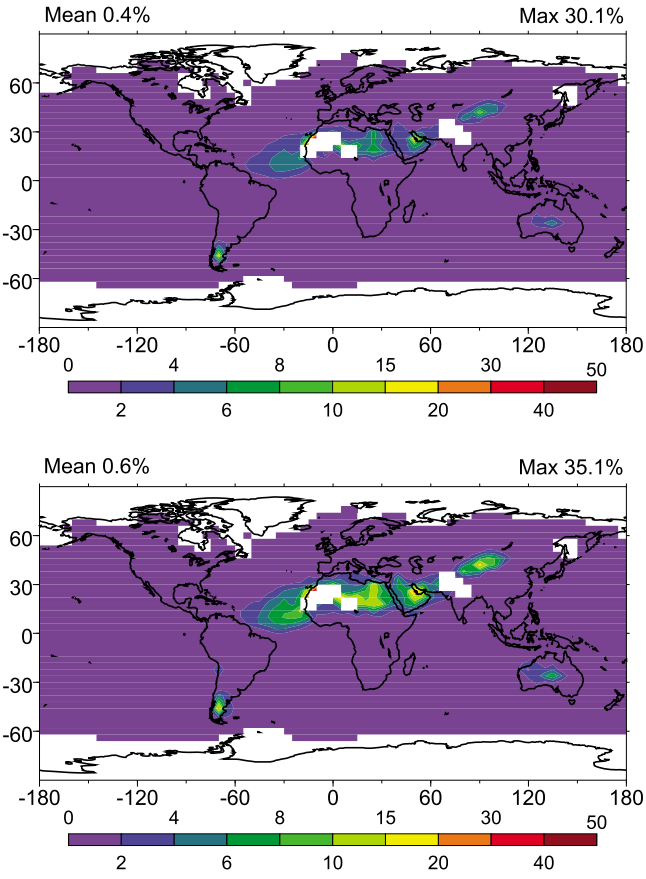

Figure 6. Predicted annual mean contribution (%) of mineral dust to total CCN for (top) 0.2% and (bottom) 0.4% supersaturation for the lowest cloud-forming level (960 mbar). White represents areas that are free of warm clouds throughout the year.

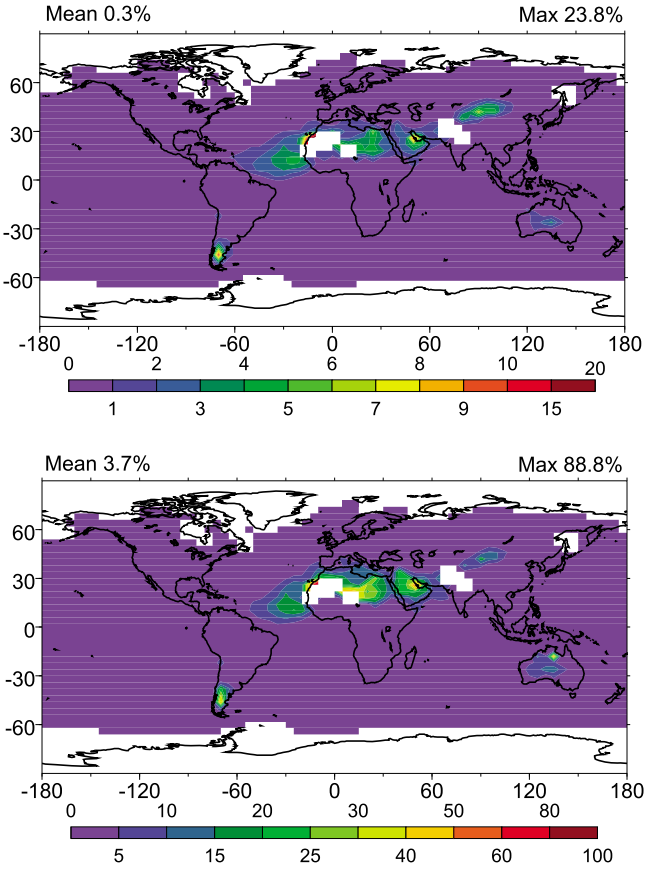

Figure 7. Predicted annual mean mineral dust contribution (%) to cloud droplet number concentration for the lowest cloud-forming level (960 mbar) by using (top) present-day and (bottom) preindustrial anthropogenic emissions. White represents areas that are free of warm clouds throughout the year.

size distribution of dust particles. To investigate the impact of uncertainty in these inputs on the predicted effect of mineral dust on CDNC, five sensitivity simulations were conducted. First, we carry out simulations using an alternate size distribution (Table 1), measured over Niger during January 2006 [*Chou et al.*, 2008]. Second, we vary the sensitivity to A_{FHH} and B_{FHH} parameters using limits reported by *Kumar et al.* [2011b]. In particular, the set of parameters used in these simulations are: A_{FHH} = 2.25, B_{FHH} = 1.1; A_{FHH} = 2.25, B_{FHH} = 1.3; A_{FHH} = 1.5, B_{FHH} = 1.2; and A_{FHH} = 3.0, B_{FHH} = 1.2. Finally, two additional sensitivity simulations were conducted to test the effect of anthropogenic emissions and atmospheric aging on mineral dust contribution to CDNC.

4.1. Sensitivity of CDNC and Total Aerosol Number to Size Distribution of Dust

[27] The size distribution used for the sensitivity test tends to distribute more mineral dust mass onto larger size particles than in the base case scenario. As a result, the number concentration of mineral dust is lower; compared to the base case simulation, the contribution of insoluble aerosols to annual mean total aerosol number concentration is found to be 45% lower (not shown). As expected, this significant change in the number of available insoluble particles reduces the contribution of dust particles to CDNC. The fraction of the droplets coming from the activation of insoluble particles is on average 23% lower than the base case simulation in areas with high concentration of dust (Table 3). Over remote areas of the Atlantic Ocean, the contribution of mineral dust to CDNC is 40% lower than the base case simulation (not shown). The base case simulation predicted that mineral dust can contribute to cloud droplet formation over a wide area that extended thousands of miles from its sources (e.g., the tropical Atlantic Ocean), in contrast to the sensitivity case simulation where the mineral dust effect on CDNC is predicted in a relatively limited area close to its sources (i.e., deserts).

4.2. Sensitivity of CDNC to A_{FHH} and B_{FHH} Parameters

[28] Lower values of the B_{FHH} parameter corresponds to a more hydrophilic particle and largely determines the existence and values of the particle critical supersaturation, s_c [*Kumar et al.*, 2009b]. A_{FHH} also affects the particle CCN activity, but to a lesser extent than B_{FHH}. *Kumar et al.* [2011b] showed that one set of the FHH parameters (A_{FHH} = 2.25 ± 0.75, B_{FHH} = 1.20 ± 0.10) encompasses the range of hygroscopicity observed for a wide range of dry-generated dust. The upper and lower bounds of this set were used as sensitivity tests in order to determine the effect of the level of hygroscopicity of dust on CDNC. When B_{FHH} = 1.3, the maximum contribution of insoluble particles to the predicted CDNC decreased to 15.1% as the mineral dust become less hygroscopic compared to the base case simulation (Table 3). Using the lower bound B_{FHH} = 1.1, almost doubled the maximum contribution of dust on CDNC to 37.2% (Table 3). The set of the FHH parameters measured by *Kumar et al.* [2011a] represents the hygroscopicity of freshly emitted dust. Nevertheless, during the aging of mineral dust, its hygroscopicity increases as it is coated with soluble materials (e.g., sea salt or sulfates), and therefore the value of 1.1 should not considered as an upper limit of hygroscopicity, as a freshly emitted dust particle with diameter 100 nm and B_{FHH} = 1.1 exhibits comparable hygroscopicity to a KT CCN with a $(NH_4)_2SO_4$ volume fraction of 10% [*Kumar et al.*, 2011a]. Finally, the results are less sensitive to changes in A_{FHH}, as the contribution of insoluble particles on the predicted CDNC varies from 17.3% (when A_{FHH} = 1.5) to 27.4% (when A_{FHH} = 3.0) with the base case value being equal to 23.8% (when A_{FHH} = 2.25; Table 3).

Table 3. Annual Mean Contribution of Mineral Dust to Cloud Droplet Number Concentrations Predicted by the Base Case and the Sensitivity Case Simulations

Simulation Scenario	Contribution
Base case	23.8%
Sensitivity to size distribution	18.0%
Sensitivity to B_{FHH} (B_{FHH} = 1.3)	15.1%
Sensitivity to B_{FHH} (B_{FHH} = 1.1)	37.2%
Sensitivity to A_{FHH} (A_{FHH} = 3.0)	27.4%
Sensitivity to A_{FHH} (A_{FHH} = 1.5)	17.3%
Sensitivity to anthropogenic emissions	88.9%

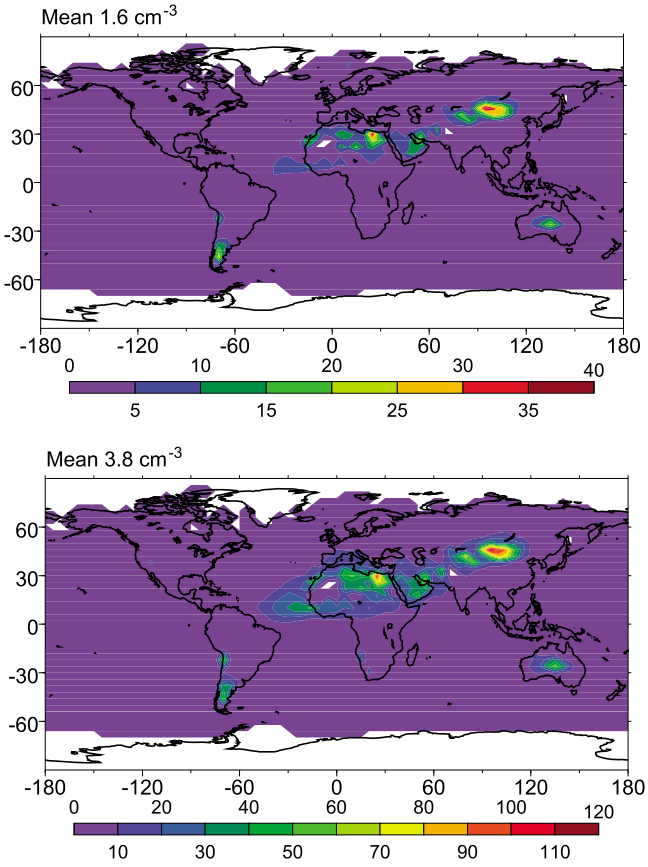

Figure 8. Predicted annual mean cloud droplet concentrations (cm^{-3}) activated from (top) completely insoluble dust particles and (bottom) aged dust particles for the lowest cloud-forming level (960 mbar).

4.3. Sensitivity of Mineral Dust Contribution to CDNC to Anthropogenic Emissions

[29] Current emission control policies are designed to lower the anthropogenic fine particulate matter concentration in order to meet the air quality standards. This will enhance the importance of mineral dust to total aerosol budget and cloud droplet formation over areas affected by anthropogenic emissions. To estimate an upper bound of mineral dust contribution to cloud droplet formation, a simulation excluding the anthropogenic emissions (emissions from fossil fuels) is conducted (pre-industrial conditions). In that case, the model predicted that close to deserts, up to 88.8% of cloud droplets formed from the activation of insoluble particles (Figure 8). On global average, the predicted contribution of mineral dust to CDNC is 12 times higher than the base case simulation (3.7% instead of 0.3% in the base case).

4.4. Sensitivity of Mineral Dust Contribution to CDNC to Atmospheric Aging

[30] During atmospheric transport, fresh dust undergoes aging, which results in a coating of soluble material on its surface that augments its CCN activity. In order to address the first order effect of aging to dust CCN activity and CDNC, a sensitivity study is conducted where dust is assumed to be coated with 10% (in volume) ammonium sulfate (called hereafter "aged dust") and it follows the same size distribution as in the base case. The "unified dust activation framework" of *Kumar et al.* [2011a] (section 2.3) is used to calculate the CCN activity of aged dust; all other parameters are kept as in the "base case" simulation. Comparison between CDNC coming from the activation of completely insoluble dust (Figure 8a) and those from aged dust particles (Figure 8b) suggests that in the latter case the contribution of dust to CDNC increased by 2.5 times on average. The maximum CDNC (predicted over the Gobi Desert) increased from 38 cm^{-3} to 115 cm^{-3}. In contrast with the completely insoluble dust particles (see section 3.3), the contribution of aged dust to CCN concentration increase with decreasing supersaturation. The increased hygroscopicity of aged dust together with its large dry diameter results in its activation at lower supersaturations than the smaller anthropogenic particles. At 0.4% supersaturation, the global annual mean contribution of mineral dust to total CCN concentration is 1% (with a maxima of 63%) while at 0.2% supersaturation the global annual mean contribution increases to 1.3% (with a maxima of 75%).

[31] Compared to freshly emitted dust, aged dust activates earlier in a cloudy updraft and grows to a larger wet size for a given supersaturation [*Kumar et al.*, 2011b]; this can promote water uptake during the initial stages of cloud formation, eventually leading to supersaturation (and CDNC) depression. This is illustrated in Figure 9, which depicts the fractional change of CDNC between a simulation assuming no activation of dust and a simulation assuming activation of aged dust. The total CDNC is decreased by as much as 70% (Gobi Desert), 60% over the Arabian Peninsula, 40% over the Sahara Desert, 20% over Australian desert, 5% over the Southwestern United States, and increased by up to 20% over the Patagonian Desert. The CDNC also decreases over a wide range of areas such as Southern Europe (up to 5%), Mediterranean Sea (up to 20%), tropical Atlantic Ocean (up to 20%), etc. As expected, s_{max} is also reduced significantly and the maximum decrease is observed over Arabian Peninsula and the Gobi Desert (up to 80%). The s_{max} decreases by up to 40% over the Sahara Desert, 30% over

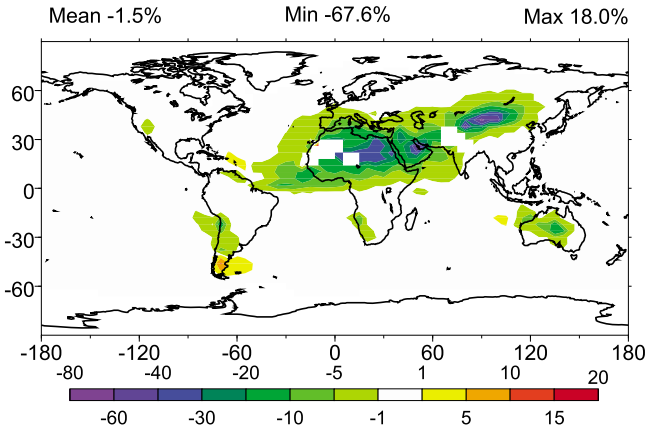

Figure 9. Predicted annual mean fractional change (%) of cloud droplet number concentration for the lowest cloud-forming level (960 mbar) between a simulation assuming no activation of mineral dust and a simulation assuming activation of aged dust.

the Australian and Patagonian deserts, 5% over the Southwestern United States and Southern Europe, 20% over the Mediterranean Sea, and 30% over the tropical Atlantic Ocean.

5. Conclusions

[32] This study is a first attempt to assess the contribution of freshly emitted insoluble dust particles to global CCN and cloud droplet number concentrations. Simulations are carried out with the NASA Global Modeling Initiative (GMI) Chemical Transport Model using wind fields computed with the Goddard Institute for Space Studies (GISS) general circulation model. GMI simulates global distributions of fossil fuel, biomass burning, marine, and dust aerosols; particles within each aerosol type are internally mixed and assumed to follow a prescribe size distribution. Particles with a significant amount of soluble material (the CCN activity of which is given by Köhler theory) are assumed to be sulfate, organic carbon, and sea salt. Dust is assumed insoluble, with the CCN activity given by adsorption activation theory; parameters required to constrain the theory are obtained from activation experiments of resuspended desert soil samples [*Kumar et al.*, 2011b]. Calculation of droplet number from the aerosol simulation is done online in GMI, using the *Kumar et al.* [2009b] parameterization, which considers cloud droplet formation within an ascending air parcel containing an external mixture of soluble particles (that activate according to Köhler theory), and insoluble, wettable particles (that form droplets through adsorption activation). This new framework is used to assess the impact of dust and adsorption activation on the predicted droplet number concentration.

[33] The contribution of mineral dust to total particle and cloud droplet number concentration is relatively important in areas with high dust concentrations (e.g., deserts) with impacts that can extend across the tropical Atlantic Ocean. The predicted contribution of mineral dust to particle number concentrations is up to 40% over North African and Asian deserts and up to 15% over South American and Australian deserts. The effect of mineral dust on the annual average CDNC is up to 23.8% while the impact on the predicted CDNC across the tropical Atlantic Ocean is up to 10% close to the shore of the Western Sahara, up to 5% to the ocean, and less that 2% to the Caribbean Sea. Given that all the results in this study are expressed as annual averages, this contribution can be even more important during specific dust storm episodes. It is worth mentioning though that the model does not account for aerosol nucleation in the upper troposphere and thus underestimates the aerosol number concentration. This underestimation also affects the influence of dust on total aerosol number concentration and consequently on CDNC.

[34] Sensitivity tests show that the results are sensitive to the level of hygroscopicity of dust, and a 10% change in the B_{FHH} parameter can lead to up to 40% change in the predicted number of activated insoluble particles. Moreover, the results are also sensitive to the size distribution of dust. Using a size distribution of dust, measured over Niger by *Chou et al.* [2008], which distributes dust in larger particles than the base case distribution (by *d'Almeida* [1987]), the predicted mineral dust particles decreased by 45% and the predicted cloud droplets activated from these insoluble particles by 20%.

[35] As current emission control policies aim to reduce the concentration of anthropogenic aerosol, the impact of dust on global aerosol budget and cloud droplet formation will become larger in the future. The theoretical upper bound of the potential contribution of mineral dust to CDNC, based on a simulation that excludes anthropogenic emissions, is up to 88.8% over regions of high dust concentrations. Coating of dust by hygroscopic aerosol species during its aging enhances its CCN activity; a sensitivity study, assuming that dust is coated with 10% ammonium sulfate (in volume), results in an increase of cloud droplets activated from dust particles (by more than twofold). This enhanced hygroscopicity leads to significant water uptake in the early stages of cloud formation, resulting in a significant depletion of s_{max} (up to 80% over arid areas and up to 30% over their surrounding areas). This large depletion also results in a significant decrease of total CDNC (up to 70 and 40% over the Gobi and Sahara deserts, respectively) but also over their surrounding areas such as Southern Europe (up to 5%), the Mediterranean Sea, and the tropical Atlantic Ocean (up to 20%). These numbers represent the first order tendency of CDNC changes; assessment of the total response of the coupled system would require an interactive aerosol-cloud-climate model and is left for a future study. Despite the sensitivities and uncertainties seen here, this study shows that dust-cloud interactions can be important. Neglecting adsorption in predicting the dust CCN activity may introduce a significant bias in the models that treat dust-cloud interactions. Given that dust may affect precipitation in climate-sensitive areas, the ability to capture the complex impact of mineral dust on cloud droplet formation is an important issue for global and regional models. This study demonstrates that a comprehensive treatment of the inherent hydrophilicity from adsorption and acquired hygroscopicity from soluble salts in dust particles is straightforward and well within the capabilities of current model frameworks.

[36] **Acknowledgments.** We would like to acknowledge support from NASA-ACMAP, ConocoPhillips, and NOAA. We are also thankful for the important comments by three anonymous reviewers, which have helped to improve the quality of the manuscript.

References

Anderson, B. E., W. B. Grant, G. L. Gregory, E. V. Browell, J. E. Collins, G. W. Sachse, D. R. Bagwell, C. H. Hudgins, B. R. Blake, and N. J. Blake (1996), Aerosols from biomass burning over the tropical South Atlantic region: Distributions and impacts, *J. Geophys. Res.*, *101*(D19), 24,117–24,137, doi:10.1029/96JD00717.

Barahona, D., and A. Nenes (2007), Parameterization of cloud droplet formation in large-scale models: Including effects of entrainment, *J. Geophys. Res.*, *112*, D16206, doi:10.1029/2007JD008473.

Barahona, D., J. Rodriguez, and A. Nenes (2010a), Sensitivity of the global distribution of cirrus ice crystal concentration to heterogeneous freezing, *J. Geophys. Res.*, *115*, D23213, doi:10.1029/2010JD014273.

Barahona, D., R. E. L. West, P. Stier, S. Romakkaniemi, H. Kokkola, and A. Nenes (2010b), Comprehensively accounting for the effect of giant CCN in cloud activation parameterizations, *Atmos. Chem. Phys.*, *10*(5), 2467–2473, doi:10.5194/acp-10-2467-2010.

Barahona, D., R. E. P. Sotiropoulou, and A. Nenes (2011), Global distribution of cloud droplet number concentration, autoconversion rate and aerosol indirect effect under diabatic droplet activation, *J. Geophys. Res.*, *116*, D09203, doi:10.1029/2010JD015274.

Bennartz, R. (2007), Global assessment of marine boundary layer cloud droplet number concentration from satellite, *J. Geophys. Res.*, *112*, D02201, doi:10.1029/2006JD007547.

Bower, K. N., et al. (1997), Observations and modelling of the processing of aerosol by a hill cap cloud, *Atmos. Environ.*, *31*(16), 2527–2543, doi:10.1016/S1352-2310(96)00317-2.

Bower, K. N., et al. (1999), The Great Dun Fell Experiment 1995: An overview, *Atmos. Res.*, *50*(3-4), 151–184, doi:10.1016/S0169-8095(98)00103-3.

Brenguier, J. L., H. Pawlowska, and L. Schuller (2003), Cloud microphysical and radiative properties for parameterization and satellite monitoring of the indirect effect of aerosol on climate, *J. Geophys. Res.*, *108*(D15), 8632, doi:10.1029/2002JD002682.

Burnet, F., and J. L. Brenguier (2007), Observational study of the entrainment-mixing process in warm convective clouds, *J. Atmos. Sci.*, *64*(6), 1995–2011, doi:10.1175/JAS3928.1.

Chen, W. T., A. Nenes, H. Liao, P. J. Adams, J. L. F. Li, and J. H. Seinfeld (2010), Global climate response to anthropogenic aerosol indirect effects: Present day and year 2100, *J. Geophys. Res.*, *115*, D12207, doi:10.1029/2008JD011619.

Chiapello, I., C. Moulin, and J. M. Prospero (2005), Understanding the long-term variability of African dust transport across the Atlantic as recorded in both Barbados surface concentrations and large-scale Total Ozone Mapping Spectrometer (TOMS) optical thickness, *J. Geophys. Res.*, *110*, D18S10, doi:10.1029/2004JD005132.

Chou, C., P. Formenti, M. Maille, P. Ausset, G. Helas, M. Harrison, and S. Osborne (2008), Size distribution, shape, and composition of mineral dust aerosols collected during the African Monsoon Multidisciplinary Analysis Special Observation Period 0: Dust and Biomass-Burning Experiment field campaign in Niger, January 2006, *J. Geophys. Res.*, *113*, D00C10, doi:10.1029/2008JD009897.

Chuang, C. C., J. E. Penner, K. E. Taylor, A. S. Grossman, and J. J. Walton (1997), An assessment of the radiative effects of anthropogenic sulfate, *J. Geophys. Res.*, *102*(D3), 3761–3778, doi:10.1029/96JD03087.

Chuang, P. Y., D. R. Collins, H. Pawlowska, J. R. Snider, H. H. Jonsson, J. L. Brenguier, R. C. Flagan, and J. H. Seinfeld (2000), CCN measurements during ACE-2 and their relationship to cloud microphysical properties, *Tellus, Ser. B*, *52*(2), 843–867, doi:10.1034/j.1600-0889.2000.00018.x.

Considine, D. B., D. J. Bergmann, and H. Liu (2005), Sensitivity of Global Modeling Initiative chemistry and transport model simulations of radon-222 and lead-210 to input meteorological data, *Atmos. Chem. Phys.*, *5*, 3389–3406, doi:10.5194/acp-5-3389-2005.

Coz, E., F. J. Gomez-Moreno, M. Pujadas, G. S. Casuccio, T. L. Lersch, and B. Artinano (2009), Individual particle characteristics of North African dust under different long-range transport scenarios, *Atmos. Environ.*, *43*(11), 1850–1863, doi:10.1016/j.atmosenv.2008.12.045.

d'Almeida, G. A. (1987), On the variability of desert aerosol radiative characteristics, *J. Geophys. Res.*, *92*(D3), 3017–3026, doi:10.1029/JD092iD03p03017.

DeMott, P. J., K. Sassen, M. R. Poellot, D. Baumgardner, D. C. Rogers, S. D. Brooks, A. J. Prenni, and S. M. Kreidenweis (2003), African dust aerosols as atmospheric ice nuclei, *Geophys. Res. Lett.*, *30*(14), 1732, doi:10.1029/2003GL017410.

Di Giuseppe, F. (2005), Sensitivity of one-dimensional radiative biases to vertical cloud-structure assumptions: Validation with aircraft data, *Q. J. R. Meteorol. Soc.*, *131*(608), 1655–1676, doi:10.1256/qj.03.129.

Dong, X. Q., and G. G. Mace (2003), Arctic stratus cloud properties and radiative forcing derived from ground-based data collected at Barrow, Alaska, *J. Clim.*, *16*(3), 445–461, doi:10.1175/1520-0442(2003)016<0445:ASCPAR>2.0.CO;2.

Dong, X. Q., T. P. Ackerman, E. E. Clothiaux, P. Pilewskie, and Y. Han (1997), Microphysical and radiative properties of boundary layer stratiform clouds deduced from ground-based measurements, *J. Geophys. Res.*, *102*(D20), 23,829–23,843, doi:10.1029/97JD02119.

Dong, X. Q., T. P. Ackerman, and E. E. Clothiaux (1998), Parameterizations of the microphysical and shortwave radiative properties of boundary layer stratus from ground-based measurements, *J. Geophys. Res.*, *103*(D24), 31,681–31,693, doi:10.1029/1998JD200047.

Dong, X. Q., P. Minnis, T. P. Ackerman, E. E. Clothiaux, G. G. Mace, C. N. Long, and J. C. Liljegren (2000), A 25-month database of stratus cloud properties generated from ground-based measurements at the Atmospheric Radiation Measurement Southern Great Plains Site, *J. Geophys. Res.*, *105*(D4), 4529–4537, doi:10.1029/1999JD901159.

Dong, X. Q., P. Minnis, and B. K. Xi (2005), A climatology of midlatitude continental clouds from the ARM SGP Central Facility: Part I: Low-level cloud macrophysical, microphysical, and radiative properties, *J. Clim.*, *18*(9), 1391–1410, doi:10.1175/JCLI3342.1.

Ekman, A. M. L. (2002), Small-scale patterns of sulfate aerosol climate forcing simulated with a high-resolution regional climate model, *Tellus, Ser. B*, *54*(2), 143–162, doi:10.1034/j.1600-0889.2002.00282.x.

Feingold, G., W. R. Cotton, S. M. Kreidenweis, and J. T. Davis (1999), The impact of giant cloud condensation nuclei on drizzle formation in stratocumulus: Implications for cloud radiative properties, *J. Atmos. Sci.*, *56*(24), 4100–4117, doi:10.1175/1520-0469(1999)056<4100:TIOGCC>2.0.CO;2.

Field, P. R., O. Mohler, P. Connolly, M. Kramer, R. Cotton, A. J. Heymsfield, H. Saathoff, and M. Schnaiter (2006), Some ice nucleation characteristics of Asian and Saharan desert dust, *Atmos. Chem. Phys.*, *6*, 2991–3006, doi:10.5194/acp-6-2991-2006.

Fountoukis, C., and A. Nenes (2005), Continued development of a cloud droplet formation parameterization for global climate models, *J. Geophys. Res.*, *110*, D11212, doi:10.1029/2004JD005591.

Fountoukis, C., et al. (2007), Aerosol-cloud drop concentration closure for clouds sampled during the International Consortium for Atmospheric Research on Transport and Transformation 2004 campaign, *J. Geophys. Res.*, *112*, D10S30, doi:10.1029/2006JD007272.

Gibson, E. R., K. M. Gierlus, P. K. Hudson, and V. H. Grassian (2007), Generation of internally mixed insoluble and soluble aerosol particles to investigate the impact of atmospheric aging and heterogeneous processing on the CCN activity of mineral dust aerosol, *Aerosp. Sci. Technol.*, *41*(10), 914–924, doi:10.1080/02786820701557222.

Ginoux, P., M. Chin, I. Tegen, J. M. Prospero, B. Holben, O. Dubovik, and S.-J. Lin (2001), Sources and distributions of dust aerosols simulated with the GOCART model, *J. Geophys. Res.*, *106*, 20,255–20,273, doi:10.1029/2000JD000053.

Grini, A., G. Myhre, C. S. Zender, and I. S. A. Isaksen (2005), Model simulations of dust sources and transport in the global atmosphere: Effects of soil erodibility and wind speed variability, *J. Geophys. Res.*, *110*, D02205, doi:10.1029/2004JD005037.

Guibert, S., J. R. Snider, and J. L. Brenguier (2003), Aerosol activation in marine stratocumulus clouds: 1. Measurement validation for a closure study, *J. Geophys. Res.*, *108*(D15), 8628, doi:10.1029/2002JD002678.

Gultepe, I., and G. A. Isaac (2002), Effects of air mass origin on Arctic cloud microphysical parameters for April 1998 during FIRE.ACE, *J. Geophys. Res.*, *107*(C10), 8029, doi:10.1029/2000JC000440.

Gultepe, I., G. A. Isaac, and K. B. Strawbridge (2001), Variability of cloud microphysical and optical parameters obtained from aircraft and satellite remote sensing measurements during RACE, *Int. J. Climatol.*, *21*(4), 507–525, doi:10.1002/joc.582.

Gultepe, I., G. A. Isaac, J. Key, J. Intrieri, D. O. Starr, and K. B. Strawbridge (2004), Dynamical and microphysical characteristics of Arctic clouds using integrated observations collected over SHEBA during the April 1998 FIRE.ACE flights of the Canadian Convair, *Meteorol. Atmos. Phys.*, *85*(4), 235–263, doi:10.1007/s00703-003-0009-z.

Harshvardhan, S. E. Schwartz, C. M. Benkovitz, and G. Guo (2002), Aerosol influence on cloud microphysics examined by satellite measurements and chemical transport modeling, *J. Atmos. Sci.*, *59*(3), 714–725, doi:10.1175/1520-0469(2002)059<0714:AIOCME>2.0.CO;2.

Henning, S., E. Weingartner, S. Schmidt, M. Wendisch, H. W. Gaggeler, and U. Baltensperger (2002), Size-dependent aerosol activation at the high-alpine site Jungfraujoch (3580 m asl), *Tellus, Ser. B*, *54*(1), 82–95, doi:10.1034/j.1600-0889.2002.00299.x.

Henrich, F., H. Siebert, E. Jakel, R. A. Shaw, and M. Wendisch (2010), Collocated measurements of boundary layer cloud microphysical and radiative properties: A feasibility study, *J. Geophys. Res.*, *115*, D24214, doi:10.1029/2010JD013930.

Herich, H., T. Tritscher, A. Wiacek, M. Gysel, E. Weingartner, U. Lohmann, U. Baltensperger, and D. J. Cziczo (2009), Water uptake of clay and desert dust aerosol particles at sub- and supersaturated water vapor conditions, *Phys. Chem. Chem. Phys.*, *11*(36), 7804–7809, doi:10.1039/b901585j.

Herman, G. F., and J. A. Curry (1984), Observational and theoretical studies of solar radiation in arctic stratus clouds, *J. Clim. Appl. Meteorol.*, *23*(1), 5–24, doi:10.1175/1520-0450(1984)023<0005:OATSOS>2.0.CO;2.

Hobbs, P. V., and A. L. Rangno (1998), Microstructures of low and middle-level clouds over the Beaufort Sea, *Q. J. R. Meteorol. Soc.*, *124*(550), 2035–2071, doi:10.1002/qj.49712455012.

Hoose, C., U. Lohmann, R. Erdin, and I. Tegen (2008a), The global influence of dust mineralogical composition on heterogeneous ice nucleation in mixed-phase clouds, *Environ. Res. Lett.*, *3*(2), 025003, doi:10.1088/1748-9326/3/2/025003.

Hoose, C., U. Lohmann, R. Bennartz, B. Croft, and G. Lesins (2008b), Global simulations of aerosol processing in clouds, *Atmos. Chem. Phys.*, *8*(23), 6939–6963, doi:10.5194/acp-8-6939-2008.

Hoppel, W. A., G. M. Frick, J. Fitzgerald, and R. E. Larson (1994), Marine boundary-layer measurements of new particle formation and the effects

nonprecipitating clouds have on aerosol-size distribution, *J. Geophys. Res.*, *99*(D7), 14,443–14,459, doi:10.1029/94JD00797.

Iacobellis, S. F., and R. C. J. Somerville (2006), Evaluating parameterizations of the autoconversion process using a single-column model and Atmospheric Radiation Measurement Program measurements, *J. Geophys. Res.*, *111*, D02203, doi:10.1029/2005JD006296.

Jeong, G. R., and I. N. Sokolik (2007), Effect of mineral dust aerosols on the photolysis rates in the clean and polluted marine environments, *J. Geophys. Res.*, *112*, D21308, doi:10.1029/2007JD008442.

Kallos, G., A. Papadopoulos, P. Katsafados, and S. Nickovic (2006), Trans-atlantic Saharan dust transport: Model simulation and results, *J. Geophys. Res.*, *111*, D09204, doi:10.1029/2005JD006207.

Kallos, G., M. Astitha, P. Katsafados, and C. Spyrou (2007), Long-range transport of anthropogenically and naturally produced particulate matter in the Mediterranean and North Atlantic: Current state of knowledge, *J. Appl. Meteorol. Climatol.*, *46*(8), 1230–1251, doi:10.1175/JAM2530.1.

Karyampudi, V. M., and T. N. Carlson (1988), Analysis and numerical simulations of the Saharan air layer and its effect on easterly wave disturbances, *J. Atmos. Sci.*, *45*(21), 3102–3136, doi:10.1175/1520-0469(1988)045<3102:AANSOT>2.0.CO;2.

Karyampudi, V. M., et al. (1999), Validation of the Saharan dust plume conceptual model using Lidar, Meteosat, and ECMWF data, *Bull. Am. Meteorol. Soc.*, *80*(6), 1045–1075, doi:10.1175/1520-0477(1999)080<1045:VOTSDP>2.0.CO;2.

Kelly, J. T., C. C. Chuang, and A. S. Wexler (2007), Influence of dust composition on cloud droplet formation, *Atmos. Environ.*, *41*(14), 2904–2916, doi:10.1016/j.atmosenv.2006.12.008.

Koch, D., and D. Rind (1998), Beryllium 10/beryllium 7 as a tracer of stratospheric transport, *J. Geophys. Res.*, *103*(D4), 3907–3917, doi:10.1029/97JD03117.

Koehler, K. A., S. M. Kreidenweis, P. J. DeMott, M. D. Petters, A. J. Prenni, and C. M. Carrico (2009), Hygroscopicity and cloud droplet activation of mineral dust aerosol, *Geophys. Res. Lett.*, *36*, L08805, doi:10.1029/2009GL037348.

Komppula, M., H. Lihavainen, V. M. Kerminen, M. Kulmala, and Y. Viisanen (2005), Measurements of cloud droplet activation of aerosol particles at a clean subarctic background site, *J. Geophys. Res.*, *110*, D06204, doi:10.1029/2004JD005200.

Kumar, P., A. Nenes, and I. N. Sokolik (2009a), Importance of adsorption for CCN activity and hygroscopic properties of mineral dust aerosol, *Geophys. Res. Lett.*, *36*, L24804, doi:10.1029/2009GL040827.

Kumar, P., I. N. Sokolik, and A. Nenes (2009b), Parameterization of cloud droplet formation for global and regional models: Including adsorption activation from insoluble CCN, *Atmos. Chem. Phys.*, *9*(7), 2517–2532, doi:10.5194/acp-9-2517-2009.

Kumar, P., I. N. Sokolik, and A. Nenes (2011a), Measurements of cloud condensation nuclei activity and droplet activation kinetics of wet processed regional dust samples and minerals, *Atmos. Chem. Phys.*, *11*(16), 8661–8676, doi:10.5194/acp-11-8661-2011.

Kumar, P., I. N. Sokolik, and A. Nenes (2011b), Cloud condensation nuclei activity and droplet activation kinetics of fresh unprocessed regional dust samples and minerals, *Atmos. Chem. Phys.*, *11*(7), 3527–3541, doi:10.5194/acp-11-3527-2011.

Lafon, S., I. N. Sokolik, J. L. Rajot, S. Caquineau, and A. Gaudichet (2006), Characterization of iron oxides in mineral dust aerosols: Implications for light absorption, *J. Geophys. Res.*, *111*, D21207, doi:10.1029/2005JD007016.

Lance, S., A. Nenes, and T. A. Rissman (2004), Chemical and dynamical effects on cloud droplet number: Implications for estimates of the aerosol indirect effect, *J. Geophys. Res.*, *109*, D22208, doi:10.1029/2004JD004596.

Lathem, T. L., P. Kumar, A. Nenes, J. Dufek, I. N. Sokolik, M. Trail, and A. Russell (2011), Hygroscopic properties of volcanic ash, *Geophys. Res. Lett.*, *38*, L11802, doi:10.1029/2011GL047298.

Leaitch, W. R., G. A. Isaac, J. W. Strapp, C. M. Banic, and H. A. Wiebe (1992), The relationship between cloud droplet number concentrations and anthropogenic pollution - observations and climatic implications, *J. Geophys. Res.*, *97*(D2), 2463–2474.

Lee, Y. H., K. Chen, and P. J. Adams (2009), Development of a global model of mineral dust aerosol microphysics, *Atmos. Chem. Phys.*, *9*(7), 2441–2458, doi:10.5194/acp-9-2441-2009.

Lehmann, K., H. Siebert, and R. A. Shaw (2009), Homogeneous and inhomogeneous mixing in cumulus clouds: Dependence on local turbulence structure, *J. Atmos. Sci.*, *66*(12), 3641–3659, doi:10.1175/2009JAS3012.1.

Leibensperger, E. M., W. T. Chen, J. H. Seinfeld, A. Nenes, P. J. Adams, D. G. Streets, N. Kumar, and D. Rind (2011), Climatic effects of 1950–2050 changes in US anthropogenic aerosols - Part 1: Aerosol trends and radiative forcing, *Atmos. Chem. Phys. Discuss.*, *11*, 24,085–24,125, doi:10.5194/acpd-11-24085-2011.

Levin, Z., and W. R. Cotton (Eds.) (2009), *Aerosol Pollution Impact on Precipitation: A Scientific Review*, 386 pp., Springer, Dordrecht, Netherlands.

Levin, Z., A. Teller, E. Ganor, and Y. Yin (2005), On the interactions of mineral dust, sea-salt particles, and clouds: A measurement and modeling study from the Mediterranean Israeli Dust Experiment campaign, *J. Geophys. Res.*, *110*, D20202, doi:10.1029/2005JD005810.

Lihavainen, H., et al. (2008), Measurements of the relation between aerosol properties and microphysics and chemistry of low level liquid water clouds in Northern Finland, *Atmos. Chem. Phys.*, *8*(23), 6925–6938, doi:10.5194/acp-8-6925-2008.

Liu, G. S., H. F. Shao, J. A. Coakley, J. A. Curry, J. A. Haggerty, and M. A. Tschudi (2003), Retrieval of cloud droplet size from visible and microwave radiometric measurements during INDOEX: Implication to aerosols' indirect radiative effect, *J. Geophys. Res.*, *108*(D1), 4006, doi:10.1029/2001JD001395.

Liu, X. H., J. E. Penner, and M. Herzog (2005), Global modeling of aerosol dynamics: Model description, evaluation, and interactions between sulfate and nonsulfate aerosols, *J. Geophys. Res.*, *110*, D18206, doi:10.1029/2004JD005674.

Luo, Y. L., K. M. Xu, H. Morrison, G. M. McFarquhar, Z. Wang, and G. Zhang (2008), Multi-layer arctic mixed-phase clouds simulated by a cloud-resolving model: Comparison with ARM observations and sensitivity experiments, *J. Geophys. Res.*, *113*, D12208, doi:10.1029/2007JD009563.

Ma, J. Z., Y. Chen, W. Wang, P. Yan, H. J. Liu, S. Y. Yang, Z. J. Hu, and J. Lelieveld (2010), Strong air pollution causes widespread haze-clouds over China, *J. Geophys. Res.*, *115*, D18204, doi:10.1029/2009JD013065.

Manktelow, P. T., K. S. Carslaw, G. W. Mann, and D. V. Spracklen (2010), The impact of dust on sulfate aerosol, CN and CCN during an East Asian dust storm, *Atmos. Chem. Phys.*, *10*(2), 365–382, doi:10.5194/acp-10-365-2010.

Menon, S., V. K. Saxena, P. Durkee, B. N. Wenny, and K. Nielsen (2002), Role of sulfate aerosols in modifying the cloud albedo: A closure experiment, *Atmos. Res.*, *61*(3), 169–187, doi:10.1016/S0169-8095(01)00140-5.

Merikanto, J., D. V. Spracklen, K. J. Pringle, and K. S. Carslaw (2010), Effects of boundary layer particle formation on cloud droplet number and changes in cloud albedo from 1850 to 2000, *Atmos. Chem. Phys.*, *10*(2), 695–705, doi:10.5194/acp-10-695-2010.

Meskhidze, N., W. L. Chameides, A. Nenes, and G. Chen (2003), Iron mobilization in mineral dust: Can anthropogenic SO_2 emissions affect ocean productivity?, *Geophys. Res. Lett.*, *30*(21), 2085, doi:10.1029/2003GL018035.

Meskhidze, N., W. L. Chameides, and A. Nenes (2005a), Dust and pollution: A recipe for enhanced ocean fertilization?, *J. Geophys. Res.*, *110*, D03301, doi:10.1029/2004JD005082.

Meskhidze, N., A. Nenes, W. C. Conant, and J. H. Seinfeld (2005b), Evaluation of a new cloud droplet activation parameterization with in situ data from CRYSTAL-FACE and CSTRIPE, *J. Geophys. Res.*, *110*, D16202, doi:10.1029/2004JD005703.

Minnis, P., P. W. Heck, D. F. Young, C. W. Fairall, and J. B. Snider (1992), Stratocumulus cloud properties derived from simultaneous satellite and island-based instrumentation during fire, *J. Appl. Meteorol.*, *31*(4), 317–339, doi:10.1175/1520-0450(1992)031<0317:SCPDFS>2.0.CO;2.

Mitsakou, C., G. Kallos, N. Papantoniou, C. Spyrou, S. Solomos, M. Astitha, and C. Housiadas (2008), Saharan dust levels in Greece and received inhalation doses, *Atmos. Chem. Phys.*, *8*(23), 7181–7192, doi:10.5194/acp-8-7181-2008.

Morales, R., and A. Nenes (2010), Characteristic updrafts for computing distribution-averaged cloud droplet number and stratocumulus cloud properties, *J. Geophys. Res.*, *115*, D18220, doi:10.1029/2009JD013233.

Nenes, A., and J. H. Seinfeld (2003), Parameterization of cloud droplet formation in global climate models, *J. Geophys. Res.*, *108*(D14), 4415, doi:10.1029/2002JD002911.

Nenes, A., S. Ghan, H. Abdul-Razzak, P. Y. Chuang, and J. H. Seinfeld (2001), Kinetic limitations on cloud droplet formation and impact on cloud albedo, *Tellus, Ser. B*, *53*(2), 133–149, doi:10.1034/j.1600-0889.2001.d01-12.x.

Penner, J. E., J. Quaas, T. Storelvmo, T. Takemura, O. Boucher, H. Guo, A. Kirkevag, J. E. Kristjansson, and O. Seland (2006), Model intercomparison of indirect aerosol effects, *Atmos. Chem. Phys.*, *6*, 3391–3405, doi:10.5194/acp-6-3391-2006.

Portin, H. J., M. Komppula, A. P. Leskinen, S. Romakkaniemi, A. Laaksonen, and K. E. J. Lehtinen (2009), Observations of aerosol-cloud interactions at the Puijo semi-urban measurement station, *Boreal Environ. Res.*, *14*(4), 641–653.

Pringle, K. J., H. Tost, A. Pozzer, U. Poschl, and J. Lelieveld (2010a), Global distribution of the effective aerosol hygroscopicity parameter for

CCN activation, *Atmos. Chem. Phys.*, *10*(12), 5241–5255, doi:10.5194/acp-10-5241-2010.

Pringle, K. J., H. Tost, S. Message, B. Steil, D. Giannadaki, A. Nenes, C. Fountoukis, P. Stier, E. Vignati, and J. Leieved (2010b), Description and evaluation of GMXe: A new aerosol submodel for global simulations (v1), *Geosci. Model Develop.*, *3*(2), 391–412, doi:10.5194/gmd-3-391-2010.

Prospero, J. M., R. J. Charlson, V. Mohnen, R. Jaenicke, A. C. Delany, J. Moyers, W. Zoller, and K. Rahn (1983), The atmospheric aerosol system: An overview, *Rev. Geophys.*, *21*(7), 1607–1629, doi:10.1029/RG021i007p01607.

Prospero, J. M., I. Olmez, and M. Ames (2001), Al and Fe in PM 2.5 and PM 10 suspended particles in south-central Florida: The impact of the long range transport of African mineral dust, *Water Air Soil Pollut.*, *125*(1), 291–317, doi:10.1023/A:1005277214288.

Querol, X., et al. (2009), African dust contributions to mean ambient PM10 mass-levels across the Mediterranean Basin, *Atmos. Environ.*, *43*(28), 4266–4277, doi:10.1016/j.atmosenv.2009.06.013.

Radke, L. F., D. A. Hegg, J. H. Lyons, C. A. Brock, P. V. Hobbs, R. Weiss, and R. Rasmussen (1988), Airborne measurements on smokes from biomass burning, in *Aerosols and Climate*, edited by P. V. Hobbs and M. P. McCormick, pp. 411–422, A. Deepak, Hampton, Va.

Rausch, J., A. Heidinger, and R. Bennartz (2010), Regional assessment of microphysical properties of marine boundary layer cloud using the PATMOS-x data set, *J. Geophys. Res.*, *115*, D23212, doi:10.1029/2010JD014468.

Rind, D., and J. Lerner (1996), Use of on-line tracers as a diagnostic tool in general circulation model development. 1. Horizontal and vertical transport in the troposphere, *J. Geophys. Res.*, *101*(D7), 12,667–12,683, doi:10.1029/96JD00551.

Romakkaniemi, S., G. McFiggans, K. N. Bower, P. Brown, H. Coe, and T. W. Choularton (2009), A comparison between trajectory ensemble and adiabatic parcel modeled cloud properties and evaluation against airborne measurements, *J. Geophys. Res.*, *114*, D06214, doi:10.1029/2008JD011286.

Rotman, D. A., et al. (2001), Global Modeling Initiative assessment model: Model description, integration, and testing of the transport shell, *J. Geophys. Res.*, *106*(D2), 1669–1691, doi:10.1029/2000JD900463.

Sassen, K., Z. Wang, V. I. Khvorostyanov, G. L. Stephens, and A. Bennedetti (2002), Cirrus cloud ice water content radar algorithm evaluation using an explicit cloud microphysical model, *J. Appl. Meteorol.*, *41*(6), 620–628, doi:10.1175/1520-0450(2002)041<0620:CCIWCR>2.0.CO;2.

Saxena, V. K., P. A. Durkee, S. Menon, J. Anderson, K. L. Burns, and K. E. Nielsen (1996), Physico-chemical measurements to investigate regional cloud climate feedback mechanisms, *Atmos. Environ.*, *30*(10-11), 1573–1579, doi:10.1016/1352-2310(95)00453-X.

Schüller, L., R. Bennartz, J. Fischer, and J. L. Brenguier (2005), An algorithm for the retrieval of droplet number concentration and geometrical thickness of stratiform marine boundary layer clouds applied to MODIS radiometric observations, *J. Appl. Meteorol.*, *44*(1), 28–38, doi:10.1175/JAM-2185.1.

Seisel, S., C. Borensen, R. Vogt, and R. Zellner (2005), Kinetics and mechanism of the uptake of N2O5 on mineral dust at 298 K, *Atmos. Chem. Phys.*, *5*, 3423–3432, doi:10.5194/acp-5-3423-2005.

Sokolik, I. N., D. M. Winker, G. Bergametti, D. A. Gillette, G. Carmichael, Y. J. Kaufman, L. Gomes, L. Schuetz, and J. E. Penner (2001), Introduction to special section: Outstanding problems in quantifying the radiative impacts of mineral dust, *J. Geophys. Res.*, *106*(D16), 18,015–18,027, doi:10.1029/2000JD900498.

Solomos, S., G. Kallos, J. Kushta, M. Astitha, C. Tremback, A. Nenes, and Z. Levin (2011), An integrated modeling study on the effects of mineral dust and sea salt particles on clouds and precipitation, *Atmos. Chem. Phys.*, *11*(2), 873–892, doi:10.5194/acp-11-873-2011.

Sorjamaa, R., and A. Laaksonen (2007), The effect of H_2O adsorption on cloud drop activation of insoluble particles: A theoretical framework, *Atmos. Chem. Phys.*, *7*(24), 6175–6180, doi:10.5194/acp-7-6175-2007.

Straub, D. J., T. Lee, and J. L. Collett (2007), Chemical composition of marine stratocumulus clouds over the eastern Pacific Ocean, *J. Geophys. Res.*, *112*, D04307, doi:10.1029/2006JD007439.

Teller, A., and Z. Levin (2006), The effects of aerosols on precipitation and dimensions of subtropical clouds: A sensitivity study using a numerical cloud model, *Atmos. Chem. Phys.*, *6*, 67–80, doi:10.5194/acp-6-67-2006.

Twohy, C. H., et al. (2009), Saharan dust particles nucleate droplets in eastern Atlantic clouds, *Geophys. Res. Lett.*, *36*, L01807, doi:10.1029/2008GL035846.

vanZanten, M. C., B. Stevens, G. Vali, and D. H. Lenschow (2005), Observations of drizzle in nocturnal marine stratocumulus, *J. Atmos. Sci.*, *62*(1), 88–106, doi:10.1175/JAS-3355.1.

Wilcox, E. M., G. Roberts, and V. Ramanathan (2006), Influence of aerosols on the shortwave cloud radiative forcing from North Pacific oceanic clouds: Results from the Cloud Indirect Forcing Experiment (CIFEX), *Geophys. Res. Lett.*, *33*, L21804, doi:10.1029/2006GL027150.

Yin, Y., and L. Chen (2007), The effects of heating by transported dust layers on cloud and precipitation: A numerical study, *Atmos. Chem. Phys.*, *7*, 3497–3505, doi:10.5194/acp-7-3497-2007.

Zender, C. S., and E. Y. Kwon (2005), Regional contrasts in dust emission responses to climate, *J. Geophys. Res.*, *110*, D13201, doi:10.1029/2004JD005501.

Zhao, C. S., et al. (2006), Aircraft measurements of cloud droplet spectral dispersion and implications for indirect aerosol radiative forcing, *Geophys. Res. Lett.*, *33*, L16809, doi:10.1029/2006GL026653.

D. Barahona, NASA Goddard Space Flight Center, 8800 Greenbelt Rd., Greenbelt, MD 20771, USA.

V. A. Karydis, A. Nenes, and I. N. Sokolik, School of Earth and Atmospheric Sciences, Georgia Institute of Technology, 311 Ferst Dr., Atlanta, GA 30332, USA. (athanasios.nenes@gatech.edu)

P. Kumar, SABIC Innovative Plastics, 1 Noryl Ave., Selkirk, NY 12158-9765, USA.